Characterization guided unit operations approach to the synthesis of Pt-Fe/SiO_2 catalysts by co-impregnation for the combustion of methane

Carol Bibiana Espinosa Lobo

Trabajo De Grado Presentado Para Optar Al Título De Magíster En Ingeniería Química

Director:
Víctor Gabriel Baldovino Medrano
Doctor en ingeniería química

Codirector:

Edwing Alexander Velasco Rozo

Magister en ingeniería química

Universidad Industrial De Santander

Facultad de ingenierías fisicoquímicas

Escuela de ingeniería química

Maestría en ingeniería química

Bucaramanga

2021

Table of Contents

List of figures

List of Tables

List of Appendices

Resumen

Título: Enfoque de operaciones unitarias guiadas por caracterización para la síntesis de catalizadores de Pt-Fe/SiO_2 por co-impregnación para la combustión de metano*

Autor: Carol Bibiana Espinosa Lobo**

Palabras claves: Combustión de metano, catalisis heterogénea, catalizador bimetálico, Pt-Fe.

Descripción: El método de síntesis se diseñó desde las operaciones unitarias involucradas en la impregnación y tratamiento térmico de los materiales. Se obtuvieron catalizadores Pt - Fe con dos tamaños de partícula de platino. Se determinó que la relación molar de los catalizadores no tuvo efecto sobre la porosidad y área específica. Sin embargo, la incorporación de los metales al soporte tuvo un efecto neto de reducción del área específica. El método de síntesis mostró alta reproducibilidad y control del tamaño de partícula metálica. El tamaño de partícula de platino determinó el comportamiento catalítico en la combustión de metano. El análisis cinético de los materiales permitió establecer que la energía de activación de la combustión de metano fue constante, para los catalizadores bimetálicos PtFe/SiO_2 pero mayor en comparación con la presentada por los catalizadores monometálicos Pt/SiO_2. Por otro lado, se estableció que la cinética de la reacción puede describirse mediante una expresión: $r_{CH4} = k_{App}[CH_4]\,[O_2]^{-0.3}$. En este caso, el valor negativo para el orden aparente de reacción de O_2 indicó que un aumento del comburente reduce la eficiencia de los catalizadores. Finalmente, fue posible establecer que existe un efecto sinérgico entre el platino y el hierro cuando la temperatura de reacción fue de 390 °C.

---

*Trabajo de investigación de Maestría en Ingeniería Química

** Facultad de Ingenierías Fisicoquímicas. Escuela de Ingeniería Química. Director: Víctor Gabriel Baldovino Medrano, Dr. Co-director: Edwing Alexander Velasco Rozo, Mg

Abstract

Title: Characterization guided unit operations approach to the synthesis of Pt-Fe/SiO_2 catalysts by co-impregnation for the combustion of methane*

Author: Carol Bibiana Espinosa Lobo**

Keywords: Methane combustion, heterogeneous catalysis, bimetallic catalyst, Pt-Fe.

Description: The synthesis method was designed from the unit operations involved in the impregnation and heat treatment of the materials. Pt-Fe catalysts with two platinum particle sizes were obtained. It was determined that the molar ratio of the catalysts had no effect on porosity and specific area. However, the incorporation of metals to the support had a net effect of reducing the specific area. The synthesis method showed high reproducibility and control of the metal particle size. The platinum particle size determined the catalytic behavior in the combustion of methane. The kinetic analysis of the materials allowed to establish that the activation energy of the methane combustion was constant, for the bimetallic PtFe/SiO_2 catalysts, but higher compared to that presented by the monometallic Pt/SiO_2 catalysts. On the other hand, it was established that the kinetics of the reaction can be described by an expression: $r_{CH4} = kApp\ [CH_4]\ [O_2]^{-0.3}$. In this case, the negative value for the apparent order of reaction of O_2 indicated that an increase in the oxidizer reduces the efficiency of the catalysts. Finally, it was possible to establish that there is a synergistic effect between platinum and iron when the reaction temperature in the reactor was 390 °C.

---

* Graduate research work to obtain the degree of Master in Chemical Engineering

** Faculty of Physico-chemical Engineering. Chemical Engineering School. Advisor: Víctor Gabriel Baldovino Medrano, PhD. Co-advisor: Edwing Alexander Velasco Rozo, Mgs

Introduction

In heterogeneous catalysis, it is necessary to obtain the largest possible metallic surface area since only the metal surface is available to catalyze the reaction. For this purpose, small metallic (crystals) of approximately 1 to 10 nm are often synthesized and dispersed over an oxide matrix (support) with high surface area. The method of preparation of supported catalysts plays a very important role in their activity, selectivity, and lifespan[1]. Highly active and selective supported metallic catalysts typically share the following features:1. Narrow metal nanoparticle size distributions, 2. High dispersion (defined as the fraction of metallic atoms present on the surface) of the metal phase over the support, and 3. Adequate metal-support interaction[2].

Taking these criteria into account, among the existing preparation methods (wet impregnation, dry or incipient impregnation, deposition precipitation, colloidal), the method that uses electrostatic adsorption for the impregnation of metals stands out. In this method, electrostatic interactions between a given metal precursor and the selected oxide support are induced by controlling the pH of the impregnation step. Starting from the point of zero charge (PZC) of the support, i.e., the pH at which the surface hydroxyls of the oxide support have no net electric charge, when the pH of an aqueous suspension of the support is below the PZC of the latter its surface hydroxyls tend to be protonated hence the surface of the suspended solid acquires a net positive charge. Conversely, when the pH of the suspension is above the PZC the hydroxyls of the support tend to deprotonate hence the surface of the suspended oxide acquires a net negative charge. The impregnation processes based on this principle tend to produce metallic supported catalysts whose mean metal particle sizes with lower standard deviations than those made without consideration of the above principle [3].

Another point in favor of pH control during the impregnation step is the possible elimination of the need for a calcination step after impregnation. Calcination can have several purposes. One of these is to eliminate impurities such as volatile and unstable anions and cations that are introduced during impregnation and, if the final objective is a metallic catalyst, it is generally sought that the metal is in its oxidized form before its

reduction, thereby ensuring the anchoring of the metal to the support [4]. However, thanks to the strong metal-support interaction provided by the difference in charges, this is often necessary. The catalysts synthesized under strict pH control seek to produce metal particles without the intermediation of oxides [5,6]. The hydration sheaths and ligands attached to the metal core of the precursors are removed via reduction or drying to preserve the highly dispersed metal particles as show in Figure 1.

Figure 1.

Hydration sheaths and ligands attached to the metal core of the precursors are removed via reduction.

Note:

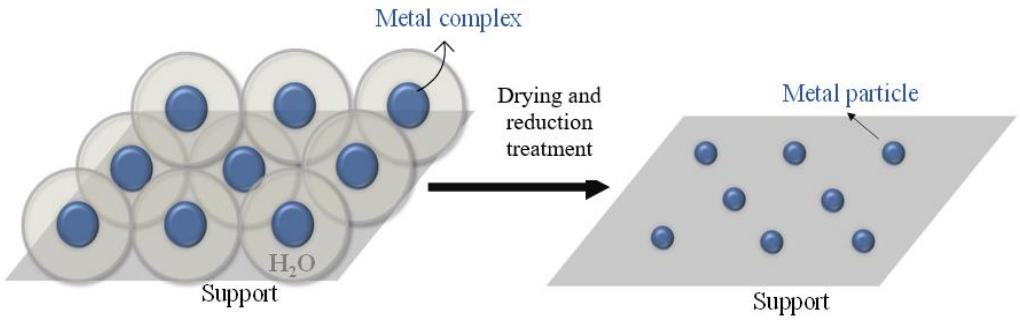

Adapted from de work of Bahareh et al. (7).

Catalytic combustion is an alternative to conventional gas flaring. The use of catalysts for the combustion of methane allows reaching conversions and selectivities towards CO_2 close to 100% at temperatures between 200 and 600°C [7–9]. Gas flaring is one of the most challenging energy, environmental, and economic problems facing the world today [10]. Flaring is used to remove excess natural gas produced in oil and gas facilities that cannot be treated for technical or economic reasons. Because this is a waste disposal process, there is no systematic report of flared gas locations and volumes [11]. Most of this gas contains high fractions of methane (84 - 97%) [12,13], hence becoming an important contributor to global warming. Indeed methane has a potential as a greenhouse gas that is approximately twenty one times higher than that of carbon dioxide [14]. On the other hand, methane is a very stable molecule, so its combustion via flaring requires temperatures above 1000°C to break one of its C-H bonds and initiate combustion [15]. Under such conditions, the formation of harmful compounds from the partial oxidation of the impurities of the flared gas such as dioxins and nitrogen oxides is favored [16,17].

Furthermore, flaring mostly produces yellow flames which are an unmistakable sign of incomplete combustion producing significant amounts of toxic CO and soot [18].

Combustion of methane has been studied by testing different types of supported noble metal based catalysts; mainly, Pt and Pd, and transition metal oxides of V, Ce, Mn, Cr, Cu, Co, Fe, Ni and W. Supported Pt-Pd catalysts are currently the benchmark for the process due to their high activity and selectivity. However, these metals are very scarce and costly; e.g., platinum is currently traded at an average 1,085 USD/oz,[19], and they can be deactivated by chlorine and sulfur heteroatoms present in the gas stream [20,21]. Additionally, platinum catalysts have presented stability problems, which is why it has been replaced or mixed with palladium, increasing its cost [22,23]. The advantage that palladium offers is the possibility of oxidizing, maintaining its activity and stability over time [24,25]. However, it is cost is at least three times higher than that of Pt.

A promising candidate to replace palladium in supported Pd-Pt catalysts for methane combustion is iron. Iron, which is currently priced at 50 USD/oz [26]; i.e. 250 times cheaper than platinum, has been used as a support of noble metals promoting the formation of single atom [27,28] and helping to improve their stability and resistance to poisoning [29-31] [17].

In particular, supported PtFe catalysts have shown excellent catalytic results in the oxidation of CO [32,33] and methanol [34–36] attributed to the strong intermetallic interaction which is considered an alloy. Chai [34] propose that the electrostatic force induced during impregnation was the reason for the formation of the PtFe alloy and concluded that this simple strategy of pH control would allow to achieve higher yields for supported noble metal catalysts that are selectively loaded over metal oxide supports.

An important fact is that Pt-Fe catalysts synthesized under pH control have not been tested for the combustion of methane. Considering the above, this work focused on the following: 1. Developing an impregnation method to produce silica supported Pt-Fe catalysts as based on an analysis of the unit operations involved in the impregnation process. 2. To analyze the functionalities of the Pt-Fe active phase for the combustion of methane.

1. Experimental

1.1 Materials

Na-SiO_2 microspheres (commercial grade, Brazilian origin) were used for obtaining the SiO_2 support of the catalysts. Iron (III) nitrate nonahydrate ($Fe(NO_3)_3 \cdot 9H_2O$, Merk, 99.95%) and tetraammineplatinum (II) nitrate ($[Pt(NH_3)_4](NO_3)_2$, Aldrich, 99.995%) were used as metallic precursors. Other materials used for the synthesis and characterization of the catalysts and for the methane combustion tests were: nitric acid (HNO_3, 65%), Sodium chloride (NaCl, Aldrich, 99.5%), Hydrochloric acid (HCl, 37%), Sodium hydroxide (NaOH, 50%), sodium nitrate ($NaNO_3$, Aldrich, 99.995%), sulfuric acid (H_2SO_4, Merck, 95-97%), hydrofluoric acid (HF, Merck, 40%), air (Linde, dry grade), nitrogen (N_2, grade 4.8, Cryogas S.A.), argon (Ar, Cryogas S.A, grade 5.0), oxygen (O_2, Cryogas, grade 5.0), methane (CH_4, Cryogas, Grade 4.0), carbon monoxide (CO, Cryogas, Grade 4.0), and hydrogen (H_2, Linde, Grade 5.0).

1.2 Pretreatment of the SiO_2 support

To eliminate sodium from the Na-SiO_2 microspheres, this solid was washed in a beaker with a 1M HNO_3 solution for 4 h at 70 °C and under 100 rpm magnetic stirring. The suspension was filtered using a filtration assembly provided with a vacuum pump while washing with deionized water until the filtered solution had a pH equal to 7. The slurry recovered by filtration was dried for 24 h at 120 °C and then roasted at 450 °C in a static oven for 4 h. The removal of Na from the SiO_2 support was verified by collecting X-ray photoelectron spectroscopy spectra before and after the procedure, see Figure S1.

1.3 Synthesis of the catalysts

The characterization route followed allows to know the conditions that promote the electrostatic interaction between the precursors and the surface of the support. Pt-Fe/SiO_2 co-impregnation was carried out at 70 °C, 200 rpm and pH equal to ~11 to avoid the precipitation of unwanted iron compounds, metal load was kept constant at 90 mmol/g and 5 Pt/Fe ratios were tested. The impregnation was kept under stirring until the solution

evaporated around 50% of its total. After impregnating the supports, the solids were filtered and dried at 100 °C in a static oven for 12 h. The synthesis for each catalyst was tripled. The catalysts were named from the following nomenclature: Pt(X)-Fe(1-X)/SiO_2-Y; Where, X is the platinum metal molar fraction and Y is the replication number.

1.4 Materials characterization

The properties of the SiO_2 support that are key for the impregnation of the metals are its point of zero charge (PZC), its distribution of surface hydroxyls, and its surface area.

The PZC of the SiO_2 support was measured by adapting the procedure proposed by Mahmood et al.[37] For PZC assessment, 180 mL of a 0.01 M NaCl solution were prepared and distributed in six (6) beakers. Then, the pH of the NaCl solutions was adjusted in a range between 1 and 11 using either HCl or NaOH solutions. pH was measured with a research grade pH-meter from HANNA instruments. Subsequently, 90 mg of SiO_2 were added to each beaker. The obtained suspensions were left under stirring at room temperature during 24 h. Afterwards, their pH was measured. Two replicas of this measurement were made.

The distribution and quantification of the surface hydroxyls of the SiO_2 support were assessed by potentiometric titration. Experiments were made at room temperature (~30.0 °C) with a LiteSizer 500 instrument from Anton Paar coupled to a Metrohm automatic titrator with an 856 conductivity module, 867 pH module, and an 846 dosing interface. An automatic titration routine was programmed via the Kalliope™ software of the instrument. The pH range for the measurements was between 3 and 11. For the experiments, ~1.0000 g of SiO_2 were suspended and equilibrated with 50 ml of a 0.05 M $NaNO_3$ solution. Then, 0.05 mL of NaOH solution were added to the suspension and left to stabilize for 15s.

The porosity and surface area of the materials were estimated from adsorption-desorption isotherms of N_2 measured at 77K. Data were recorded in the relative pressure range (P/P_0) between 0.0025 and ~0.9900 using an equilibration time of 10 s. Isotherms were measured with a 3FLEX® instrument (Micromeritics). Before the analyses, approximately 0.2900 g of sample were degassed under vacuum at 120 °C for 1 h and then

at 300 °C for 12 h. The duration of the outgassing procedure was defined after finding that the vacuum in the cells reached ca. 0.05 mbar. The weight of the outgassed samples was recorded and used as input data for recording the adsorption-desorption isotherms. The surface area was calculated by the Brunaeur-Emmett-Teller (BET) method[38]; The pore volume (Vp) and the pore diameter (Dp) were calculated with the Barrett-Joyner-Halenda (BJH) method assuming that the pores had a cylindrical geometry using the MicroActive® software provided with the instrument. The values of the BET area of the catalysts reported were estimated by selecting those point of the isotherms that optimized the BET C constant according to the method proposed by Rouquerol[39,40] which is provided by the software of the instrument.

The loadings of platinum and iron of the catalysts were measured by atomic absorption. For the measurements, samples from the materials were dried for 1 h at 120°C in a 100 mL/min flow of air before the analyses. The digestion of the samples was done following the protocol proposed by Westerman *et al*. For this purpose, ca. 0.5000 g of the samples were transferred into a polytetrafluoroethylene beaker where they were put in contact with a mixture of 2 to 5 mL of sulfuric acid and 5 mL of hydrofluoric acid under heating at 70°C. The procedure was stopped when sulfur trioxide fumes appeared since this indicates that silica has been completely dissolved and that the excess hydrofluoric acid has been evaporated. The cooled digests were diluted to 100 mL with deionized water and stored in polythene jars for performing the atomic absorption tests.

The thermogravimetric profiles of the materials were recorded with a TGA 2050 thermogravimetric balance (TA Instruments) whose precision is ± 0.1 wt.%. For the tests, samples were placed in a platinum sample holder and heated from 25 °C to 1000 °C, heating ramp: 10 °C/min, under a static N_2 atmosphere. An analysis of the compounds desorbed during this procedure was made by performing an analogous heating routine in a CATLAB system coupled to a QGA® mass spectrometer -MS- (Hiden Analytical). The QGA-MS was equipped with both an internal dual electron multiplier detector, SEM, and a Faraday detector, and with a precision quartz inlet heated capillary sampling interface. In this case, ~0.4000 g of sample was placed in the quartz reactor (0.7 cm i.d.) and heated under a 50 mL/min gas flow from 40 °C to 800 °C, heating ramp: 5 °C/min. The CATLAB

instrument was also used for recording the compounds desorbed from the fresh catalyst under flows of Ar.

The hydrogen temperature–programmed reduction (TPR) profiles of the catalysts were recorded with the same CATLAB instrument mentioned above. For the measurements, samples of ~0.1500 g were used. TPR profiles were recorded between 40°C and 800°C, heating rate: 5 °C/min, under a 50 mL/min flow of a 5 vol% mixture of H_2 in Ar. Before the analysis, samples were dried under a flow of 50 mL/min of Ar at 120°C for 1h and then at 300°C for another 3h. The reduction process was followed by monitoring the MS signals for H_2, H_2O, Ar, CH_4, CO and CO_2. The consumption of hydrogen during the experiments was below the detection limits of the MS (RSF=0.48[42]). Therefore, the analyzes were made following the water production signal. A deconvolution of the peaks from the TPR profiles was made with Fityk® software using the Gaussian function[43].

The dispersion of the metallic phases of the catalysts was estimated by independent CO and O_2 chemisorption tests using the CATLAB instrument previously described. Prior to the measurements, the samples were heated at 100 °C under vacuum, cooled to room temperature and pretreated with an H_2 stream at 200 °C for 1 h. Chemisorption tests made over samples of the monometallic catalysts showed Pt/SiO_2 chemisorbed CO and not O_2, while Fe/SiO_2 chemisorbed O_2 but not CO, Figure S10. Therefore, it was assumed that independent CO and O_2 chemisorption experiments were suitable for determining the concentration of exposed platinum and iron sites, respectively, in the bimetallic catalysts. For platinum, a stoichiometry of one mole of platinum per mole of CO was assumed [44], while a stoichiometry of two moles of iron per mole of O_2 was assumed [45]. Metallic particle sizes were estimated using the standard assumption that particles are hemispheres [46]. The instrument was calibrated with pulses of 15µL of the CO/Ar and O_2/Ar mixture for quantification purposes. Chemisorption measurement were replicated thrice by taking independent samples of the catalysts.

1.5 Catalytic tests

Catalysts were tested in the combustion of methane. Tests were carried out in a quartz fixed bed reactor (1.1 cm i.d.) at atmospheric pressure (1.0 atm). Samples of ca.

0.2000 g of each catalyst were used. The reactor was filled by introducing the catalyst sample in the middle of two glass wool beds and two quartz tubes, as shown below:

Figure 2.

Reactor packing system for catalytic tests

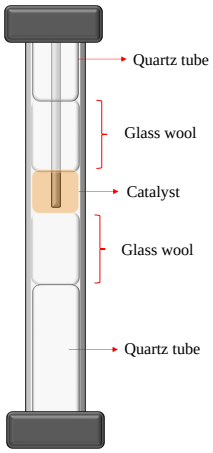

Before starting the catalytic tests, the samples were dried under a 3.568 mmol/min flow of N_2 at 120°C for 1h and then at 300°C for 3h. Afterwards, the catalysts were reduced with a 0.1784 mmol/min flow of H_2 at 200 °C for 1 h. The reaction conditions were set after ruling out mass transport limitations. Methods and results of these tests are described in the Supplementary Information, Section D.

The reactions were carried maintaining the stoichiometric ratio CH_4/O_2 in 1:2, the particle diameter used was between 180-300 mm and a weight of feed per hour per unit weight of catalyst loaded in the reactor (WHSV) of 35 $Lg^{-1}h^{-1}$. The CH_4, O_2 and N_2 fluxes were constant with values of 0.4460, 0.8920 and 3.5680 mmol/min, respectively.

First series of catalytic tests were done with the aim of analyzing the thermal stability of the catalysts. These tests were made by rising the temperature from 300 to 500°C and then back to 300°C with randomly selected temperature steps. A second series of stability tests were made within the temperature range from 350 to 390 ° C, the same conditions of the preliminary temperature tests were implemented.

The reproducibility of the catalytic tests was checked by carrying out two and three replicates of them with randomly selected catalysts (Table S6), average values are reported.

An additional set of experiments were done for the catalyst Pt(0.25)Fe(0.75)/SiO_2-1 keeping the temperature fixed at 350°C for the catalyst. For these tests, the reactor was operated in a differential mode with conversion of CH_4 always below 10%. Therefore, reaction rates were calculated assuming the model of a continuous stirred tank reactor (CSTR) [47,48]. Under these conditions, an additional On the other hand, apparent reaction orders and apparent activation energies were estimated. Assuming that the plug flow reactor is operating at a low enough conversion that the velocity through the catalyst bed is invariant and therefore can be approximated as a CSTR, the kinetic analysis was limited to the study of the reaction order in terms of the reactants, the possible inhibition by H_2O, CO and CO_2 was not taken into account as they did not exceed the limit for which it is considered (> 3-5 kPa)[49].

The analysis of the reactor effluent was made on–line with a GC–2014 chromatograph (Shimadzu) equipped with 80/100 Hayesep Q (300cm) and 60/80 Mol–Sieve 5A (300cm) packed columns, and a thermal conductivity detector (TCD) coupled to a methanizer and to a flame ionization detector (FID). The methanizer consists of a Ni catalyst bed that transforms CO and CO_2 into CH_4 ($CO_x + (2+x)H_2 \rightarrow CH_4 + xH_2O$) at 375°C for their indirect detection in the FID. For the analyses, the temperature of the columns of the instrument was kept at 100°C using argon as carrier (20mL.min^{-1}). Meanwhile, the TCD and FID detectors were operated at 160 and 200 °C, respectively. All gases were fed to the reactor via mass flow controllers (Alicat) whose accuracy was ±0.1% of their full scale. The operating pressure was set at the reactor outlet using a back–pressure regulator (Alicat) with an accuracy of ±0.3% of its full scale. The temperature of the system was monitored in the catalytic bed and close to the external wall of the reactor with K thermocouples enclosed within stainless–steel 316 sheets (3.175 mm o.d.). The temperature of the oven was set and controlled with a programmable logic controller (Rockwell) whose accuracy was ± 1°C. The difference between the recorded temperatures in the bed and the external wall of the reactor was kept lower than 5°C. For all tests, N_2 was used as diluent of the gas mixtures fed to the reactor. The products detected during the reaction tests were CO_2, CO, CH_4, O_2 and H_2O. The calibration of these compounds was made by injecting gas

mixtures of known composition to the GC and results are show in Supplementary information Section D. The following equations were used for quantification:

$$F_i = b_i \cdot \frac{A_{i,TCD}}{A_{N_2,TCD}} \cdot F^0_{N_2} \quad \text{Equation 1}$$

$$F_j = \frac{b_j}{a_j} \cdot \frac{A_{i,FID}}{A_{N_2,TCD}} \cdot F^0_{N_2} \quad \text{Equation 2}$$

Where, $F_{i \text{ or } j}$ is the estimated molar flow; F^0_{N2} is the inlet N_2 molar flow; $A_{i \text{ or } j}$ is the chromatographic peak area of the corresponding analyte either in the TCD or FID; $b_{i \text{ or } j}$ is the response factor for each analyte; and a_j is a proportionality factor between the FID and TCD peak areas. The method implemented for quantifying the effluents from the reactor is presented in detail elsewhere[50,51]. On all occasions, it was confirmed that the mass balance for carbon would close with a value of 1 (Table S6). Finally, the composition of the gas mixture fed to the reactor was quantified with the mixture at room temperature at the end of the corresponding reaction tests.

1.6 Expression of the catalytic results

Conversion and selectivity were calculated from the following equations:

$$X_{CH_4} = \frac{F^{in}_{CH_4} - F^{out}_{CH_4}}{F^{in}_{CH_4}} \quad \text{Equation 3}$$

$$Sp_i = \frac{mol\ p_i}{\sum_i mol\ p_i} \quad \text{Equation 4}$$

Where, $F^{in}_{CH_4}$ is the inlet molar flow rate of CH_4 [mol CH_4/s], $F^{out}_{CH_4}$ is the methane molar flow in the product stream [mol CH_4/s] and p_i is CO_2 or CO.

When the reactor was operated in the differential mode, apparent reaction rate ($r_{CH4,App}$) were estimated according to the following equation:

$$r_{CH_4,App} = \frac{F^{in}_{CH_4} \cdot X_{CH_4}}{N} \text{ [=] } s^{-1} \quad \text{Equation 5}$$

Where, N is the number of moles of Pt in the catalyst [mol Pt], and X_{CH4} is methane conversion. In this expression, it was assumed that platinum was the catalytic active phase because under the studied reaction conditions, monometallic iron catalysts were not catalytically active.

From such rates, apparent reaction orders and apparent activation energies were estimated. The possible inhibition by H_2O, CO and CO_2 was not taken into account as they did not exceed the limit for which it is considered (> 3-5 kPa)[49], so a power law expression is defined for the rate of:

$$r_{CH_4,App} = k_{eff}\left[P_{CH_4}\right]^a\left[P_{O_2}\right]^b \qquad \text{Equation 6}$$

When k_{eff} is the effective rate constant, $[P_{CH4}]$ y $[P_{O2}]$ are the partial pressures of reagents and a and b are the reactions orders.

1.7 Statistic analysis

Non-linear regression analysis of experimental data was used to fit the titration curve using Microsoft EXCEL [52]. The coefficient of determination (R^2 value) calculated gave an estimate of goodness of fit of the function to the data. The error bars for the replicated experiments were calculated with confidence intervals of the Student's t test with a significance level of 5% and n-1 degrees of freedom. Catalyst deactivation at low temperature was analyzed using the paired samples t-test. Methane conversion was compared assuming that the difference between light off conversion and light out conversion was cero as null hypothesis with significance level of 5% and n-1 degrees of freedom [53]. Analysis of variance (ANOVA) was used to verify the existence of significant differences in the means for CO_2 selectivity. For this, two factors (temperature and sample) and a significance level of 5% were considered. Calculations were made with a single sample the two-ways ANOVA tool from MS EXCEL.

2. Results and discussion

2.1 Characterization guided co-impregnated of the Pt-Fe/SiO_2 catalysts

Figure 3.

Schematic methodology for the synthesis of the bimetallic catalysts Pt(x)-Fe(1-x) /SiO_2.

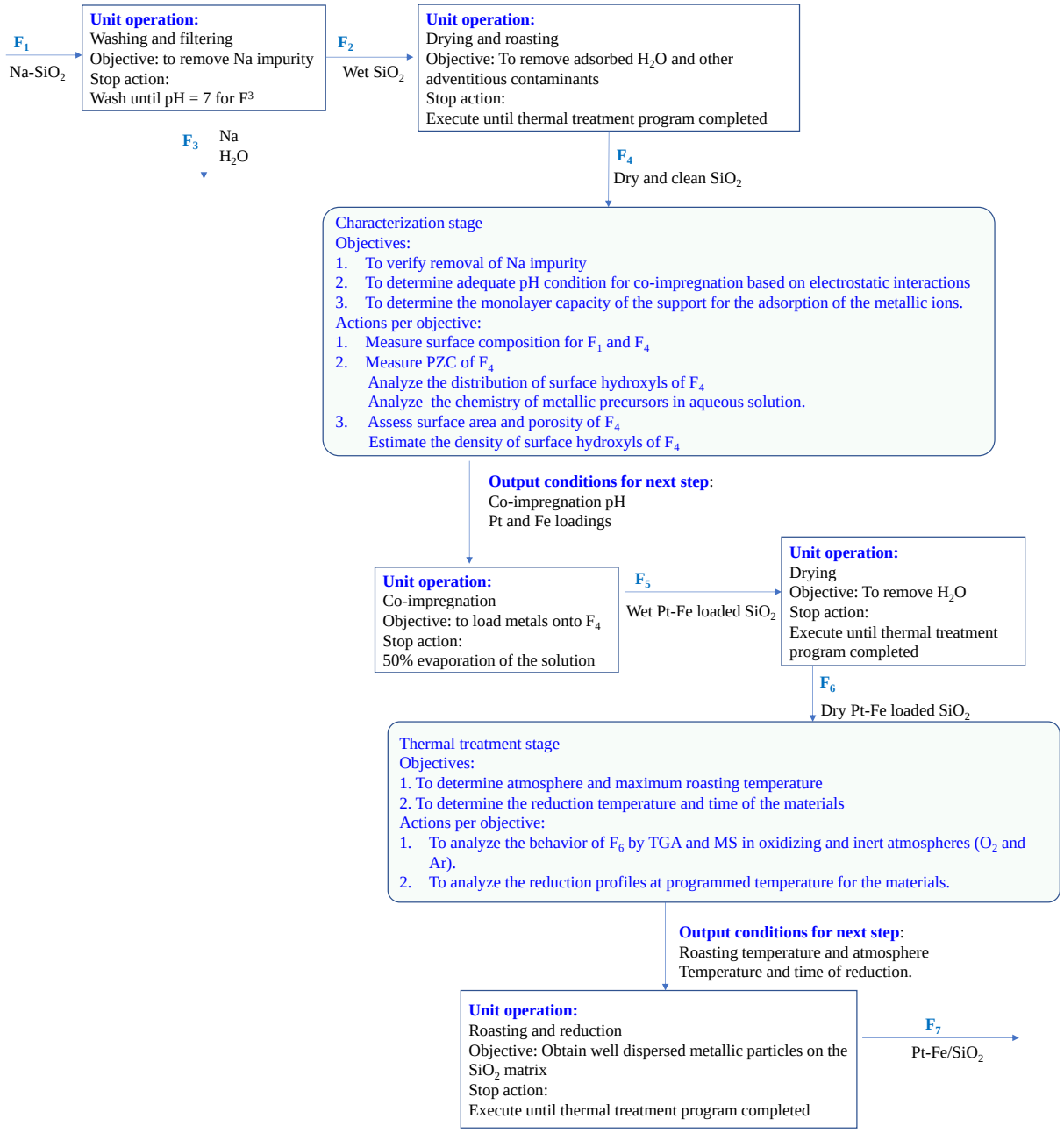

A schematic diagram with the step by step carried out for the impregnation of the catalysts is presented in Figure 3. The process was divided into two main stages and five unit operations. First, a purification stage of the support had to be carried out because the sample was contaminated with traces of sodium, after washing the recovered solids were dried and roasted, this was the starting point for the determination of the impregnation conditions and subsequent determination of the conditions of the thermal treatment for the catalysts after the impregnation.

2.1.1 Determination of impregnation conditions.

Once the total elimination of sodium from the support was confirmed, it was characterized. The results of the physicochemical characterization of SiO_2 support are shown in Table 1. The support showed a type of isotherm (Figure S2) with unrestricted adsorption at the limit $P/P_0 \sim 1.0$ and a wide hysteresis loop that closed near $P/P_0 \sim 0.6$. This type of isotherm is not part of the IUPAC classification [40], and could be classified as a mixture of types H2 (b) and H3. An important characteristic of this silica is its low surface area; media = 19.3 ± 0.2 m^2/g. Its PZC was approximately at pH 3.5 ± 0.1 (Figure S3) and, according to the diagram for the distribution of surface hydroxyls species, Figure S6, its surface hydroxyls become partly protonated at pH below 1.4 and completely deprotonated at pH above 8.0. The estimated density of silanol groups was 5.7 OH/nm^2; which was close to the 5.0 OH/nm^2 theoretical value for silicas [54]. According to the above data, there were $5.50 \cdot 10^{20}$ OH available for forming a metallic monolayer over the SiO_2 support. Considering such monolayer capacity, the metallic loadings of the catalysts was fixed taking half of a theoretical metallic monolayer over the SiO_2 support. This translated into catalysts whose total number of moles of metal, either platinum or iron, was constant and equal to 4.6×10^{-4} mol (the calculations leading to these values are presented in the supporting information Section B).

Considering the surface charge profile for the SiO_2 support (Figure S6), it was decided that for making the co-impregnation of the metals under a regime controlled by

electrostatic interactions, the pH of the solution of the metallic precursors should be above 8.

Table 1.

Summary of the parameters and typical results from SiO_2 microspheres.

BET area [m^2/g]	19.3 ± 0.2
Pore volume [cm^3/g]	0.09
Pore diameter[nm]	25
OH/nm^2	5.697
PZC	3.50 ± 0.1
pK1	1.37
pK2	5.63

On the other hand, the metal coordination complexes formed from the precursors have charge +2 ($[Fe(NH_3)_6]^{+2}$ and $[Pt((NH_3)_4]^{+2}$). For this reason, 2 surface SiO^- sites are required for the adsorption of each complex. The reactions were adapted as follows [55–58]:

$$Fe(NO_3)_3 + 3NH_3 + 3H_2O \rightarrow 3NH_4NO_3 + Fe(OH)_3$$

$$Fe(OH)_3 + 6NH_3 \rightarrow [\boldsymbol{Fe(NH_3)_6}]^{+2} + 3OH \quad \text{Equation 7}$$

$$Pt(NH_3)_4(NO_3)_2 + 2NH_3 + 2H_2O \rightarrow 2NH_4NO_3 + [\boldsymbol{Pt(NH_3)_4}]^{+2} + 2OH \quad \text{Equation 8}$$

2.1.2 Determination of thermal treatment.

Drying and calcination stage. Figure 4 is a composite plot done from the correlation between the TGA and temperature programmed desorption analyses made for the dried solids from the previous synthesis stage. These results were characteristics for all catalysts. The total weight loss from the materials was around 3 wt.%, due to the low porosity of the material. Three regions of weight loss regions were identified in the TGA

profile; namely, one between 50–130°C, another between 150–175°C, and the las one between 275–325 °C. According to the TPD profile, the first region of weight loss corresponded to the desorption of CO_2 and physiosorbed H_2O, the second to the desorption of NH_3, and the third to the desorption of CO, CO_2, and chemisorbed H_2O. H_2O, CO, and CO_2 are mainly adsorbed by the catalyst during storage while NH_3 is a product of the decomposition of metallic precursors [59].

Figure 4.

TGA-MS curves for the selected catalyst Pt(0.75) -Fe(0.25)/SiO_2.-2.

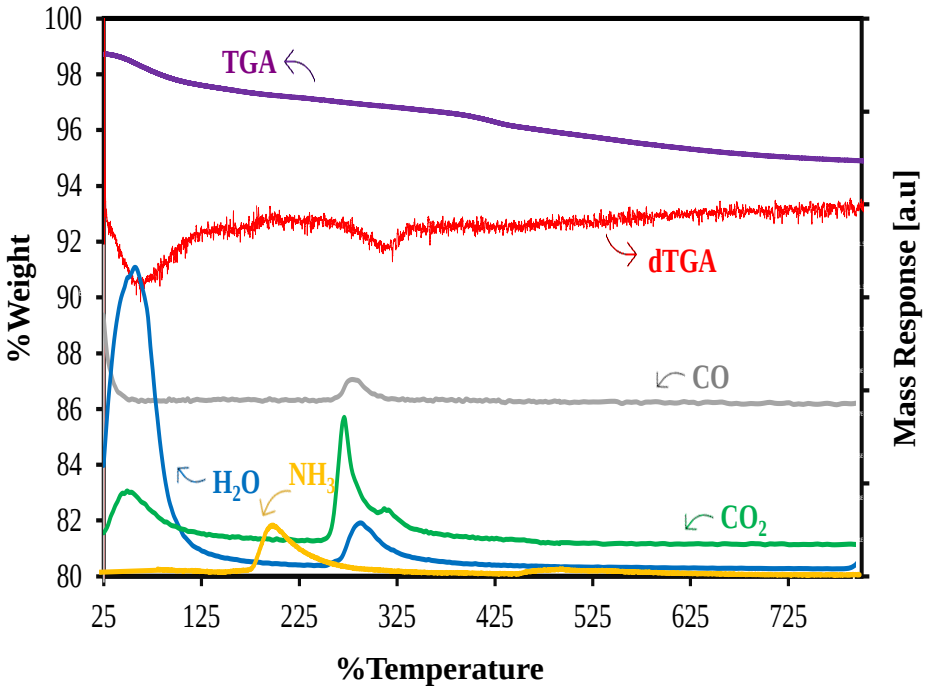

Other authors have recommended the calcination of this type of materials at 300 ° C in N_2 or Ar atmospheres to obtain better catalytic results, since for the systems studied, the increases in temperature generated the rearrangement of the metallic particles and therefore their agglomeration, which resulted in a decrease in dispersion or metallic surface [60–63]. In conclusion, temperatures above 300 ° C will not contribute to the elimination of contaminants or to the decomposition of the metallic precursors, so this will be the selected calcination temperature. Regarding the exposure time at the temperature of 300 ° C, it was set at 4 h.

Reduction stage:

Figure 5.

H_2 TPR profiles quantified by water production and peak deconvolution

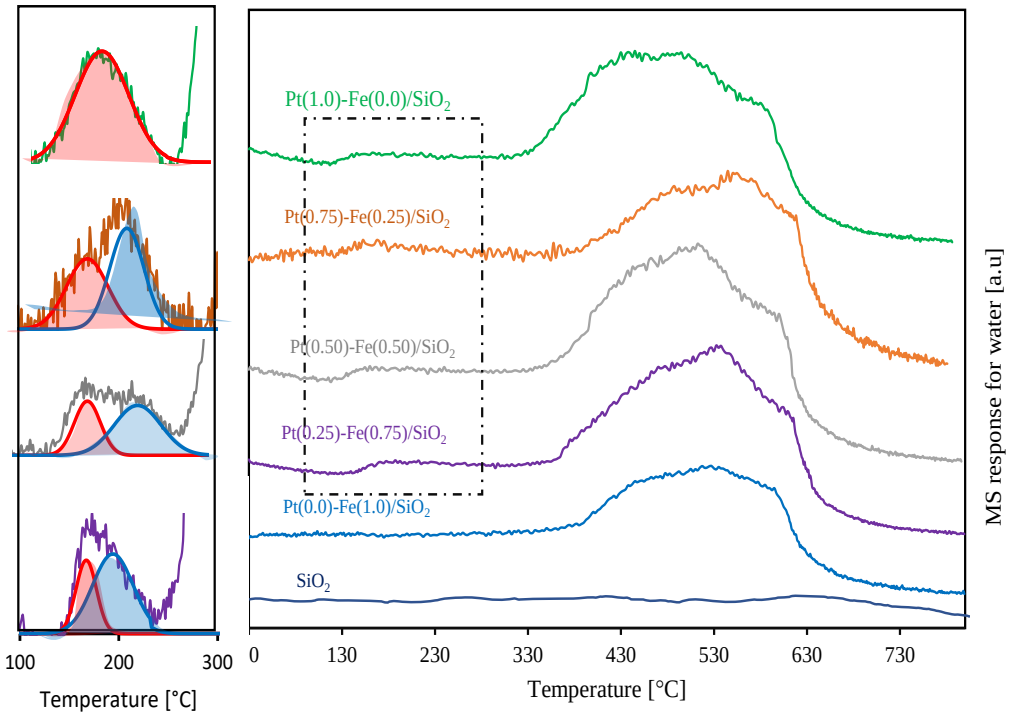

Figure 5 shows the H_2O mass response for the H_2 Temperature-programmed reduction profiles for the catalysts. Two water production peaks are observed, the first appears in all the catalysts except Pt(0.0)-Fe(1.0)/SiO_2-2 with its maximum at ~179 °C, the second widest and largest peak appears on all catalysts in the region of 450 -550 °C. An important point is that for SiO_2 no reduction peaks were observed. The peak at low temperatures represents the reduction of Pt^{+2} to Pt^0 following Equation 9 [61] and second peak supposed the reduction of iron (Equation 10) in the range of 450-550 ° C, but the presence of this peak in the catalyst with (0.0) Fe led to a deeper analysis. Furthermore, in all catalysts, CO_2 production was evidenced in the same temperature range.

$$PtO_2 + 2H_2 \rightarrow 2H_2O + Pt \qquad \text{Equation 9}$$

$$Fe_2O_3 + 3H_2 \rightarrow 3H_2O + 2Fe$$ Equation 10

The results for Pt(1.0)-Fe(0.0)/SiO_2-2 are summarized in Figure 6. In first place, the production of methane at low temperatures and its subsequent consumption to produce CO_2 and H_2O is observed, the compiled for the other catalysts is presented in Figure S7. As a hypothesis, chemisorbed CO_2 is being hydrogenated (methanated) during the test, which, favored by the high temperature, would react with the surface oxygen of the catalyst, from the following reaction route [64–66]:

$$CH_4 + O_2^{SUP} \rightarrow CO_2 + H_2O$$ Equation 11

Figure 6.

H_2-TPR for Pt(1.0)-Fe(0.0)/SiO_2-2. MS response for H_2O, CO_2 and CH_4 are shown.

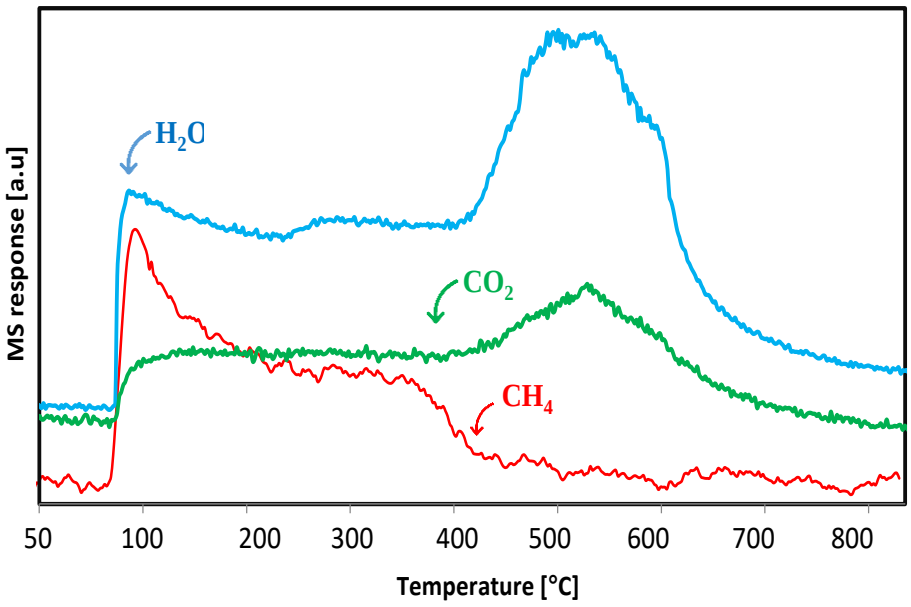

The point of interest is found in the first peak observed in H_2-TPR, which was deconvolved. The lowest temperature peak corresponds to the reduction of oxidized platinum particles and the second peak shifted to the right is attributed to the partial reduction of oxidized iron species that are bound to Pt particles, due to a possible Pt-O-Fe

interaction[67,68] (Figure 5). However, it is not possible to quantify the water production, for this reason it was implemented a calculation strategy for the comparison of the reduction profiles between the catalysts. The ratio between the areas for water production was calculated and compared in relation to the monometallic Pt catalyst by the following equation:

$$Relative\ percentage\ area\ of\ Pt = \frac{Area_{p1,i}}{Area_{P1,Pt(1.0)-\frac{Fe(0.0)}{SiO_2}}} \cdot 100 \qquad \text{Equation 12}$$

Where, $Area_{p1,i}$ is the area of the first deconvolved peak for each catalyst and $Area_{P1,Pt(1.0)-\frac{Fe(0.0)}{SiO_2}}$ is the area of Pt deconvolved for Pt(1.0)-Fe(0.0)/SiO_2.-2 . The results of the relative percentages of Pt in the catalysts are shown in Table 2. Assuming that in all cases all the impregnated platinum was reduced, an approximate error of 15% with respect to the theoretical relationships between the metals would be estimated by this comparison method. On the other hand, as expected, the A1/A2 ratio decreases when Fe load increases.

Table 2.

H_2O production at low reduction temperature for deconvolved peaks. Quantification of areas and calculation of A_1/A_2 ratio.

	Summit peak 1	Summit peak 2				
Sample	**T [°C]**	**T [°C]**	**$Area_{Peak1}$**	**$Area_{Peak2}$**	**%Relative Pt reduction**	**A1/A2**
Pt(1.0)-Fe(0.0)/SiO_2	197.5	-	4.35E-09	-	100%	-
Pt(0.75)-Fe(0.25)/SiO_2	188.1	213.2	2.61E-09	1.74E-09	60%	1.50
Pt(0.50)-Fe(0.50)/SiO_2	158.0	220.1	1.83E-09	2.52E-09	42%	0.72
Pt(0.25)-Fe(0.75)/SiO_2	190.0	213.2	8.35E-10	3.51E-09	19%	0.24
Pt(0.0)-Fe(1.0)/SiO_2	-	-	-	-	-	-

Note: Tests were done for replica 2 synthesis.

These results indicate that the reduction temperature necessary for the bimetallic system is 200 ° C, since at this temperature the total reduction of the metal particles of Pt is achieved. As for the reduction time, a reduction test at constant temperature (200°C)

allowed to determine that no more than 1 h is needed to complete the reduction (See Figure S 8).

The changes in the porosity of the synthesized materials were studied before heat treatment (fresh), after their calcination and reduced. From Figure 7**,** it can be concluded that there is no significant effect of the Pt/Fe ratio or of the heat treatment on the porosity of the catalysts, since all the data recorded are within the 95% confidence interval for silica. In addition, no type of trend is observed between the data. The decrease in the surface area of the catalysts with respect to the support could be explained considering that the metallic particles fill available spaces in the silica. However, this decrease is not significant (Section c for details).

Figure 7.

Comparative plot for the porosity of fresh, calcined, and reduced catalysts

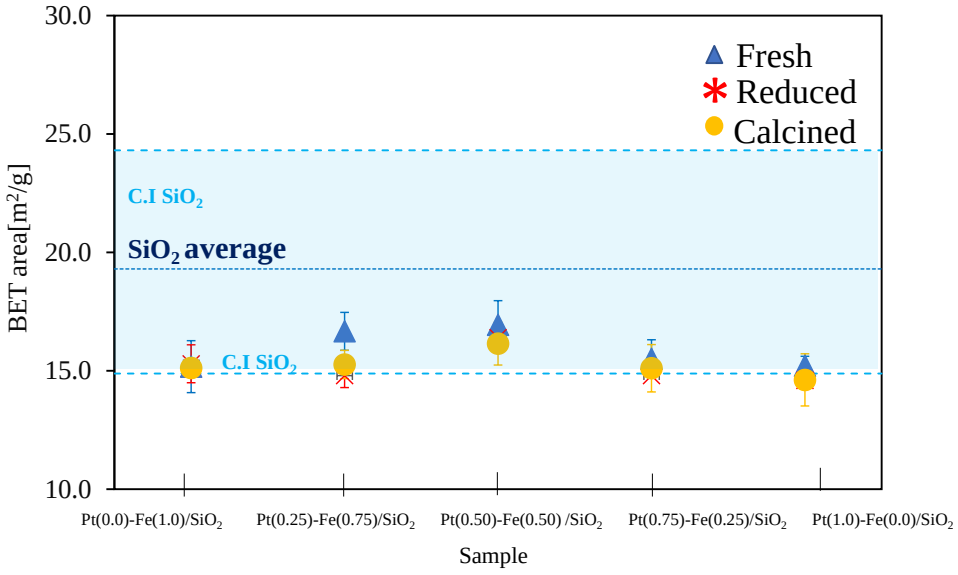

Once the conditions for the synthesis of the catalysts were fixed, an analysis of their properties was made. This analysis is presented next. In what follows, we will catalyst only to those materials produced after the reduction stage. Therefore, the properties described below belong to the state of the catalysts just before starting the catalytic tests.

2.2 Physicochemical properties of the synthesized catalysts

Metallic contents. Table 4 presents the theoretical and real metal content values obtained by atomic absorption and chemisorption. In the first place, an impregnation efficiency of around 70% in the bulk was observed, while at surface levels the impregnated metallic quantity was below 40%. An important note is that the theoretical relationship between the metals was not preserved in bulk but did maintain its proportion on the surface. This is an indication that the impregnation of each precursor was done equally and without competition for the OH sites.

Table 3.

Metal contents for PtFe catalysts

	Theoretical content [mmol/g]		Bulks content* [mmol/g]		Surface content** [mmol/g]				
Sample	Pt	Fe	Pt	Fe	Pt	Fe	Bulk ratio Pt/Fe	Theoretical ratio Pt/Fe	Surface ratio Pt/Fe
Pt(0.0)-Fe(1.0)/SiO_2	0.0	89.5	0.0	69.2	0.0	29.0	0	0	0
Pt(0.25)-Fe(0.75)/SiO_2	22.4	67.1	19.1	54.1	15.2	17.5	0.868	0.334	0.353
Pt(0.50)-Fe(0.50)/SiO_2	44.9	44.8	32.3	29.3	14.3	15.8	0.909	1.000	1.102
Pt(0.75)-Fe(0.25)/SiO_2	67.3	22.4	50.0	13.1	13.9	15.7	0.888	3.008	3.816
Pt(1.0)-Fe(0.0)/SiO_2	89.7	0.0	52.3	0.0	25.0	0.0	-	-	-

Note: *Metal contents obtained by atomic absorption. The analyzed data correspond to replica 3.

**Metal contents obtained by O_2 / CO chemisorption

Metallic dispersion and particle sizes. Regarding the dispersion of metals, an interesting observation is the inverse relationship found between the metallic fraction and the dispersion. This contradicts previous works, which showed how the increase in the number of metals particles (Metal fraction in the catalyst) produces an increase in dispersion[69] (Figure 8). However, the impregnated catalysts under pH control the seeks the selective impregnation of metal complexes on the OH groups available in the support, for this reason, one of the variables with the greatest influence on the impregnation performance is the available surface area. The error bars demonstrate the homogeneity of the catalysts because for the synthesized catalyst replicates there is no significant difference

between the results (Table S5). For catalysts with low platinum loads (0.25 and 0.75 mole fraction), values of Pt dispersion in both cases are much higher than other samples with similar composition and supports with a larger surface area reported in the literature [70,71].

Figure 8.

Comparison plot for the dispersion of Pt and Fe individually. Before analysis catalyst were calcined at 300°C for 3h in Ar atmosphere and reduced in H_2 at 200° C.

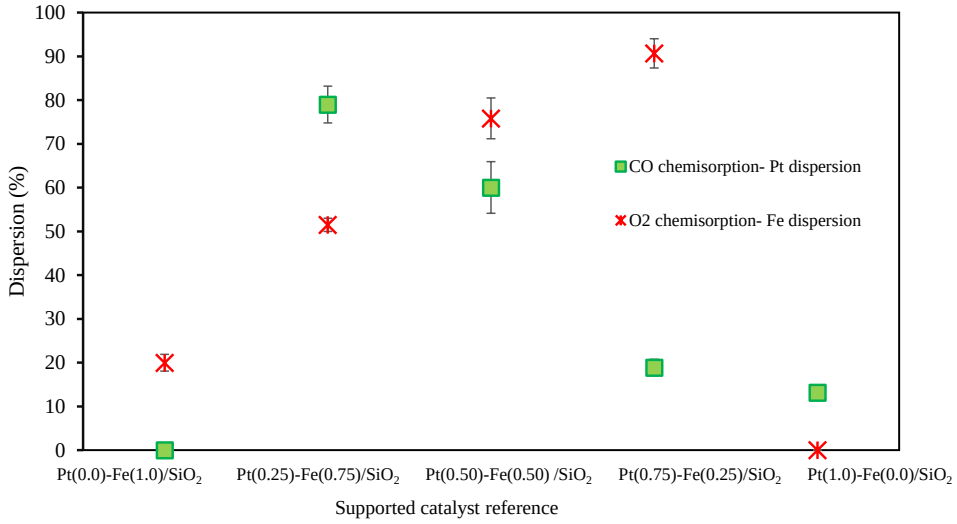

Similarly, the increase in the individual metal fraction generated an increase in the particle size (Table 3). In this case we suppose that the high percentages of individual metallic charge produced agglomeration and the formation of larger particles, this influenced by the low porosity of the support.

Table 4.

Particle size for PtFe catalysts

Sample	Pt particle size [nm]	Fe particle size [nm]
Pt(0.0)-Fe(1.0)/SiO_2	-	5.03 ± 0.46
Pt(0.25)-Fe(0.75) /SiO_2	1.27 ± 0.07	1.94 ± 0.06
Pt(0.50)-Fe(0.50) /SiO_2	1.68 ± 0.17	1.32 ± 0.08
Pt(0.75)-Fe(0.25) /SiO_2	5.32 ± 0.51	1.10 ± 0.04
Pt(1.0)-Fe(0.0) /SiO_2	7.62 ± 0.49	-

In general, Table 4 allows a comparison of the metal contents in the catalysts, from these results it is proposed that the impregnation mechanism followed two possible routes, the first influenced by the difference in charges between the precursor solution and the support. However, when the OH groups avaible were found to be occupied, the metal particles were deposited in the available pores in a disorderly manner (Figure 7). This can be explained because Chemisorption[72] is used to quantitatively measure the number of surface-active sites which are used to promote a specified catalytic reaction, while techniques such as TPR and AA allow volumetric quantification of the components of the sample.

Figure 9.

Graphical representation of the impregnation model

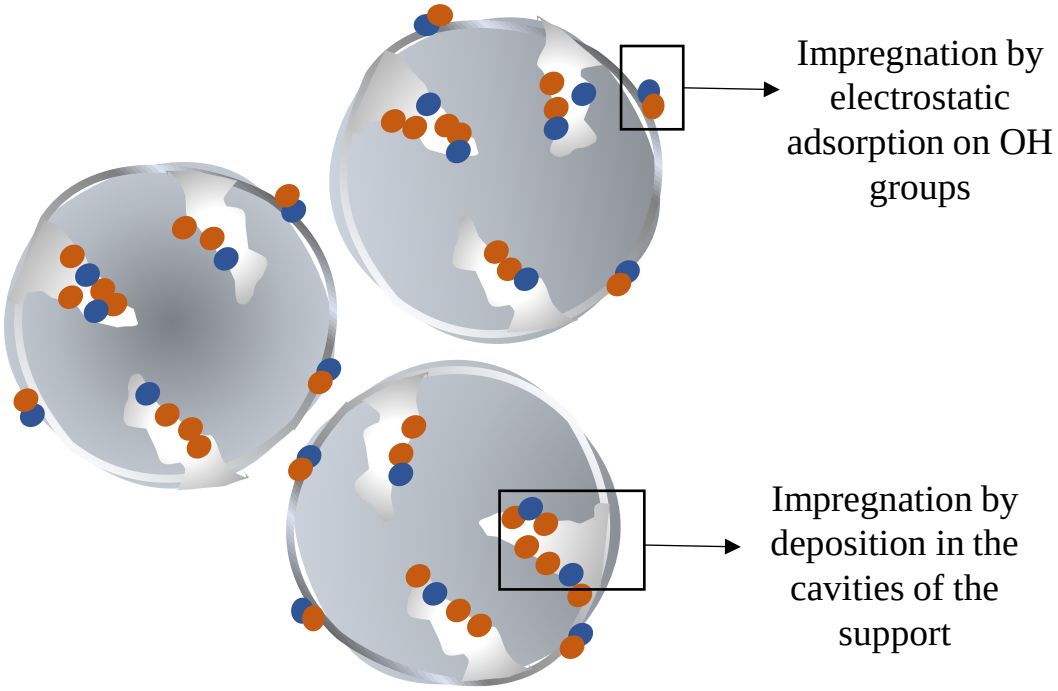

The impregnation hypothesis raised can be supported by calculating the surface area normalized (N_{ABET}).

$$N_{ABET} = \frac{A_{BET\ catalysts}}{A_{BET\ support}\left(1 - (x_{Pt} + x_{Fe})\right)} \qquad \text{Equation 13}$$

In this equation, $A_{BETcatalysts}$, is the surface area of the catalysts, $A_{BET\ support}$, the area of the support and (x_{Pt} + x_{Fe}) is the fraction of the metals. The values of N_{ABET} close to 1 suggest that the metallic phase is well dispersed in the support and therefore it does not cause pore clogging. The opposite is suggested when N_{ABET} is well below 1. The values reported in Table 5 from N_{ABET} were not very close to 1.0 (0.77-0.86), which suggests pore clogging occurred after incorporation of the metallic particles on the support.

Table 5.

Surface area normalized (N_{ABET}). Before analysis catalyst were calcined at 300°C for 3h in Ar atmosphere and reduced in H2 at 200° C.

Catalyst	A_{BET}^{*}	$(x_{Pt} + x_{Fe})$	N_{ABET}
SiO_2	19.3	0	1.000
Pt(0.0)-Fe(1.0)/SiO_2	15.3	0.0050	0.797
Pt(0.25)-Fe(0.75)/SiO_2	14.8	0.0082	0.773
Pt(0.50)-Fe(0.50)/SiO_2	16.4	0.0113	0.859
Pt(0.75)-Fe(0.25)/SiO_2	14.8	0.0144	0.778
Pt(1.0)-Fe(0.0)/SiO_2	14.6	0.0175	0.770

Note: The A_{BET} values correspond to the average for each catalyst

2.3 Catalytic performance in methane combustion

2.3.1 Characterization of the ignition and extinction behavior.

The catalysts exhibit the typical behavior expected for the combustion of hydrocarbons. At around 300 ° C, the oxidation of methane started (X_{CH4} ~ 1.0%) for all catalysts except for the catalyst with a null platinum fraction, the oxygen conversion followed the same behavior described below (Table S6). At the beginning, the temperature over the catalyst is low and thus the reaction rate is limited by the intrinsic kinetics (zone A). The increase in temperature leads to an exponential increase in speed (zone B) to the point where the heat generated by combustion is much greater than the heat supplied. Upon reaching zone C, the intrinsic reaction rate rapidly increases but gradually the mass transfer

rate cannot keep up with[16]. At high temperatures the reaction behaves like a strong and spontaneous explosion. For this reason, the kinetics of catalytic combustion is only relevant for zone A (temperatures of 300-400 °C). For the evaluated temperatures, it is observed that the catalysts with low platinum fractions did not reach zone C. Also, Figure 10 shows the hysteresis effects during ignition (light-off) and extinction (light-out) exothermic CH_4 oxidation reactions for Pt-Fe catalysts. Two behaviors were seen, firstly normal hysteresis is appreciated for catalysts with low platinum fraction (0.25 and 0.50), it is attributed to the blocking of active sites by formed intermediaries that remain adsorbed on the surface, decreasing the light-off activity[73] or morphological changes due to sintering of Pt particles. On the other hand, the catalysts containing high platinum fractions (0.75 and 1.0) showed inverse hysteresis at high temperatures. The higher activity of the catalyst during extinction can be attributed mainly to the exothermicity of the reaction and thermal inertia of the catalyst [74–76].

On the other hand, when reaching the temperature of 500 °C, the catalysts presented a strong deactivation produced by the temperature control of the system (Figure S17), demonstrated in the error bar.

Figure 10.

Light off and light out curves from 300 to 500°C.

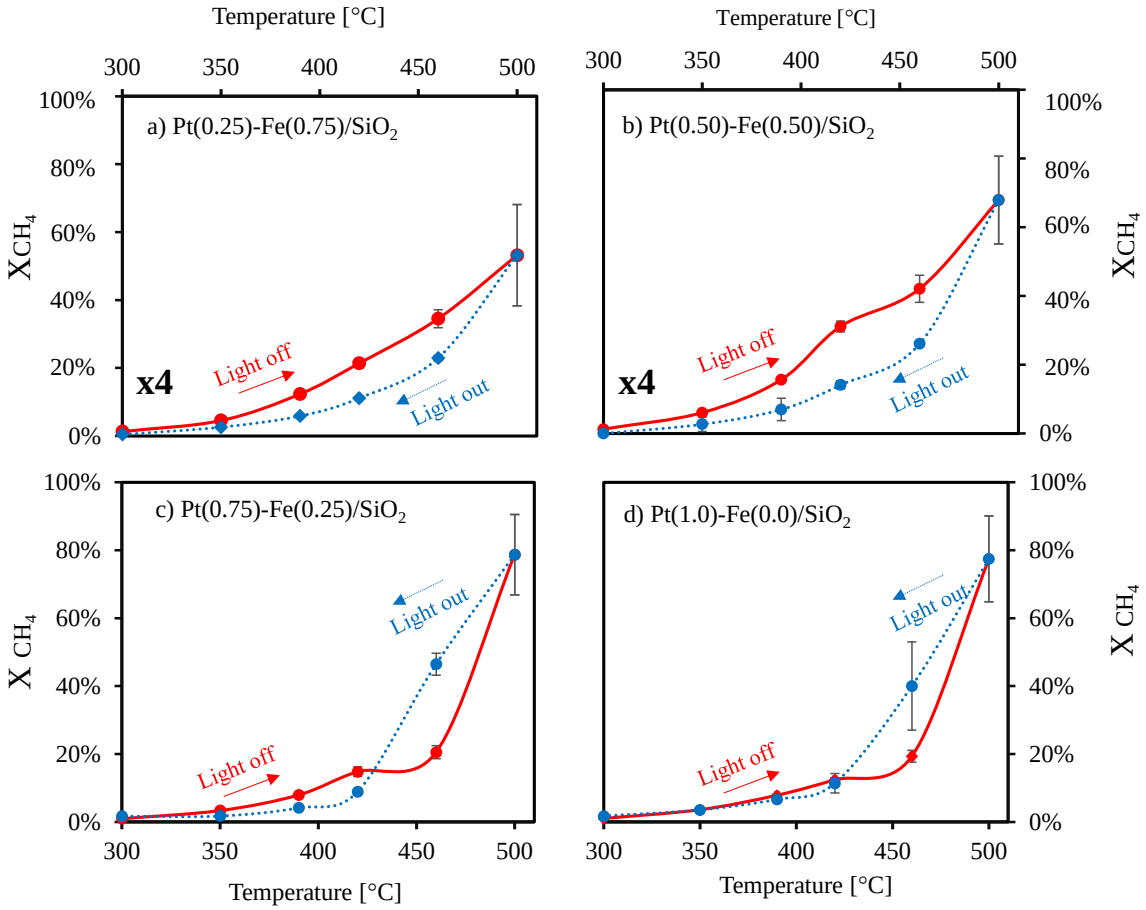

Note: Pt(0.0)-Fe(1.0) is not shown because it does not present catalytic activity. Error bars correspond to the 95% confidence interval for the average methane conversion

To avoid the limitations possibly produced by high temperature (sintering, overheating of catalyst surfaces, thermal inertia of the catalyst, among others) second set of reactions will be restricted to region between 350 to 390 ° C. Table 6 shows the new results at low temperature. To rule out catalysts deactivation, the significance level was compared to p-value in the paired t-test. For all the catalysts in the temperature range studied, the p-value remained above 0.05, except for Pt (1.0)-Fe (0.0)/SiO_2 showing a slight difference in methane conversions during ignition and extinction. These results imply that the interaction between the metals favors the stability of the catalysts.

Table 6.

Catalytic results for low temperature methane combustion and paired t-test data.

	Sample							
	Pt(0.25)-Fe(0.75)/SiO_2		Pt(0.5)-Fe(0.5)/SiO_2		Pt(0.75)-Fe(0.25)/SiO_2		Pt(1.0)-Fe(0.0)/SiO_2	
Temperature [°C]	350	370	350	370	350	370	350	370
$Mean_{Light\ out}$	0.0154	0.0217	0.0185	0.0278	0.0249	0.0379	0.0321	0.0449
Standard $deviation_{Light\ out}$	0.0011	0.0007	0.0012	0.0011	0.0010	0.0015	0.0004	0.0013
Number of $data_{Light\ out}$	8	9	8	9	8	9	8	9
$Mean_{Light\ off}$	0.0160	0.0213	0.0184	0.0286	0.0241	0.0367	0.0133	0.0288
Standard $deviation_{Light\ off}$	0.0006	0.0009	0.0015	0.0005	0.0012	0.0017	0.0001	0.0007
Number of $data_{Light\ off}$	8	9	8	9	8	9	8	9
Difference mean	-0.0006	0.0004	0.0001	-0.0008	0.0008	0.0011	0.0189	0.0162
Standard deviation of the difference	0.0010	0.0008	0.0014	0.0013	0.0012	0.0021	0.0004	0.0014
t- student	-1.5940	1.4851	0.2823	-1.8576	1.7553	1.5739	139.78	35.28
p-value	0.1550	0.1758	0.7859	0.1003	0.1226	0.1542	0.0000	0.0000
Conclusion	No difference	No difference	No difference	No difference	No difference	No difference	Difference	Difference

Figure 11 shows the direct relationship between methane conversion and selectivity towards CO_2 is clarified, since as the temperature increases, the conversion towards CH_4 will increase and therefore the selectivity towards CO_2 will be greater. ANOVA test allows a more in-depth analysis of the results, so it is possible to conclude that there is no significant difference in the CO_2 selectivity for the catalysts, while at 350 ° C a significantly different behavior than those of 370 and 390 ° C (Supplementary information section f). Although the selectivities towards CO_2 are high, the presence of CO shows that the direct oxidation route is not followed.

Figure 11.

CO_2 selectivities for the reaction test vs temperature.

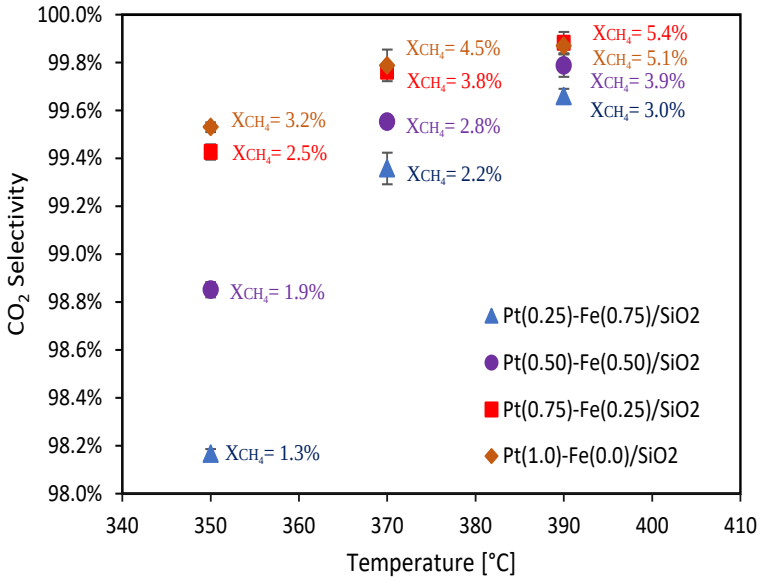

Note: For each selectivity data the corresponding methane conversion is attached. The results of the Pt (0.0)-Fe(1.0)/SiO_2-1 catalyst are not shown due to no activity. Results correspond to replica 1.

Compared with other platinum-based catalysts, those synthesized in this work presented higher conversions than others with higher compositions, for this reason, they were promoted with palladium[77]. However, in terms of selectivity, other catalysts have managed to guarantee full selectivity towards CO_2[78]. The main advantage is the possibility of achieving performance close to or better than catalysts whose metallic percentages are much higher.

2.3.2 Kinetic analysis.

The corresponding Arrhenius plot is shown in Figure 12. The apparent activation energy is significantly the same for the bimetallic catalysts (approximate estimation error of 5%) while for the platinum monometallic catalyst the value is reduced, see Table S7. According to the literature, catalytic combustion reduces the activation energy values from 100-200 kJ mol^{-1} (conventional combustion) to 40-80 kJ mol^{-1} [1][9]. However, compared to

other platinum catalysts for the combustion of methane, the catalysts developed in this work achieved lower Ea values [25].

Figure 12.

Arrhenius plot for CH_4 oxidation

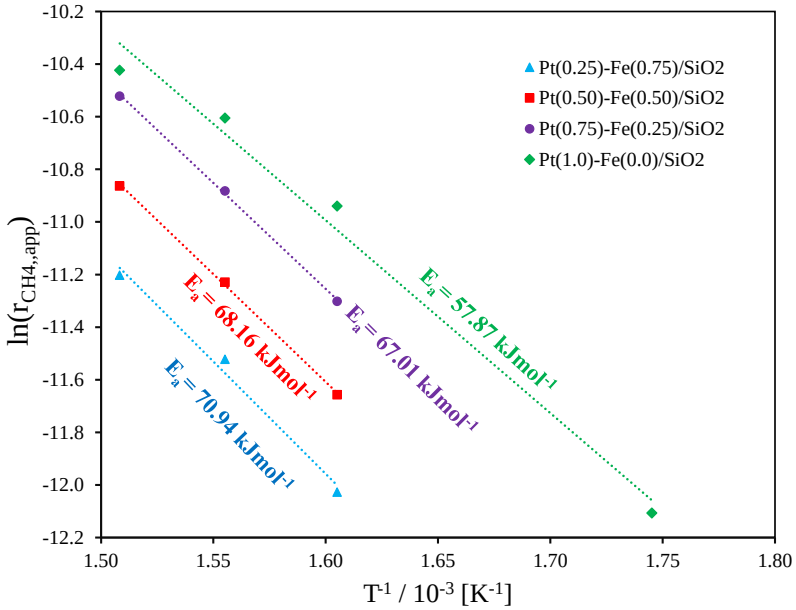

Note: One more data was added to the adjustment for the catalyst Pt (1.0)-Fe (0.0)/SiO2. The results for the catalyst Pt (0.0)-Fe(1.0)/ SiO_2 are not shown as it does not present activity. Particle diameter used was between 180-300 mm, WHSV= 35 L g^{-1} h^{-1}. The CH_4, O_2 and N_2 molar fluxes were constant with values of 0.4460, 0.8920 and 3.5680 mmol/min, respectively. The activation energy was calculated as: -slope * R[J mol^{-1} K^{-1}]. Results correspond to replica 1.

The reaction order dependence on CH_4 and O_2 was determined at 350°C for the catalyst Pt(0.25)-Fe(0.75)/SiO_2 , because, the parallelism evidenced in the Arrhenius graph allows us to select any of the bimetallic catalysts for analysis. The results are shown in Figure 13. Under these conditions, the catalytic combustion of methane on Pt-Fe catalysts is close to first order in CH_4 (1.06) and negative zero order in O_2 (-0.33). The results agree with what has been reported in the literature, the reaction is ~zero negative order in oxygen and first order in methane[16]. In this case, the negative coefficient for O_2 indicates the inhibition of the reaction due to the presence in excess of this reagent, that the adsorption of

hydrocarbons on the active sites turns out to be energetically competitive with O_2 under the conditions studied[79]. Also, the reaction order shows that the methane conversion on the PtFe catalyst does not depend on the methane concentration in the reactor feed[80].

Figure 13.

Natural log of the CH_4 oxidation rate at 350°C for Pt(0.25)-Fe(0.75)/SiO_2.

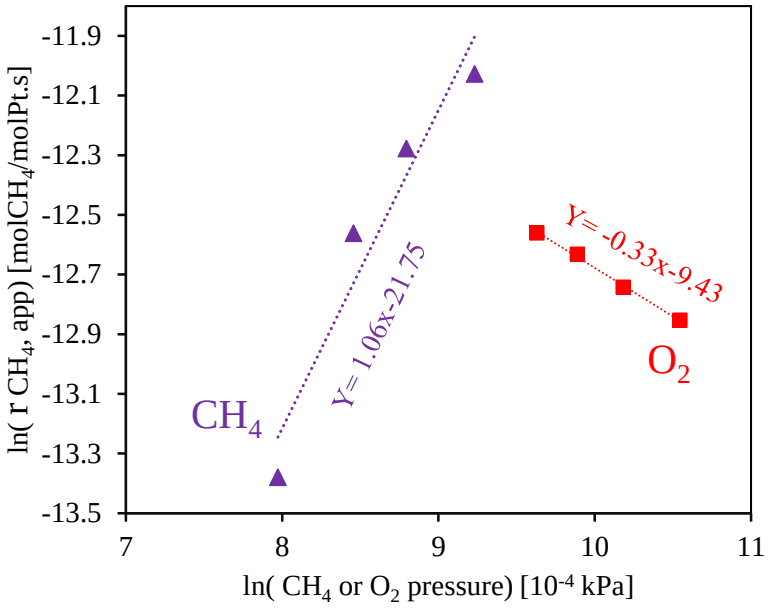

One possibility is that the metallic particles are oxidizing during the reaction which would produce a decrease in the catalytic activity and possible inhibition, to rule out this, the H_2-TPR test was repeated on the catalysts spent by reaction at 500 ° C and 350 ° C. As can be seen in Figure S18, in both cases no peaks were observed that indicate the reduction of Pt or Fe species, so that during the reaction the bimetallic catalysts remained reduced.

An important part of this study is to understand the synergy between Pt and Fe in the performance of methane combustion. Synergy is defined as a non-linear (non-additive) effect of increasing activity or selectivity upon changing concentrations of the components of the catalytic systems[81]. As shown in Figure 15, at temperatures of 350 and 370, the catalysts remain very close to the expected behavior line, however, a possible synergistic effect is presented for bimetallic catalysts at 390 °C. This can be explained considering that bimetallic catalysts reached the highest platinum dispersions and additionally, from the

hysteresis curves, we found that catalysts with high platinum fractions show a delay in their catalytic activity.

Figure 14.

Synergy graph.

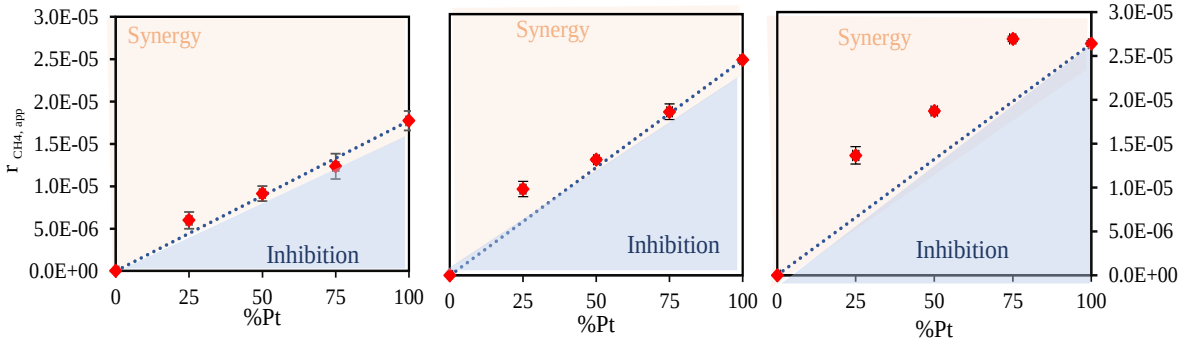

Note: The zone of synergy and inhibition are represented. a) Test at 350 ° C; b) Test at 370 ° C; c) Test at 390 ° C. Particle diameter used was between 180-300 mm, WHSV= 35 L g-1 h-1. The CH_4, O_2 and N_2 molar fluxes were constant with values of 0.446, 0.892 and 3.568 mmol/min, respectively.

3. Conclusions

PtFe catalysts were synthesized following a synthesis route guided by the characterization results, the key point was to guarantee a metal-support interaction that promoted high metal dispersion and avoided calcination of the material. In the first place, the impregnation mechanism followed two possible routes, the first influenced by the difference in charges between the precursor solution and the support, however, when the enabled OH groups were found occupied, the metallic particles were deposited in the available pores. disorderly, this due to the low surface area of the support. The reduction profiles show the possible Pt-O-Fe interaction and although it was not possible to quantify the hydrogen consumed, the relationship between deconvolved peaks shows that the relationship between metals was maintained during impregnation. The decrease in the surface area of the catalysts with respect to the support could be explained considering that the metallic particles fill available spaces in the silica, nevertheless, there is no significant effect of the Pt/Fe ratio or of the heat treatment on the porosity of the catalysts. One of the variables with the greatest influence on impregnation performance is the available surface. Because the catalysts impregnated under pH control seek the selective impregnation of metal complexes on the OH groups available in the support, this was evidenced in the increase in dispersion as the individual metal fraction increased. Finally, the homogeneity of the synthesized catalysts was demonstrated.

The catalysts showed the typical behavior expected for the combustion of hydrocarbons. The oxidation of methane started at temperatures close to 300 ° C and the apparent deactivation at high temperatures is associated to the temperature control of the reactor. The catalysts were shown to have a high selectivity towards CO_2 (> 98%) and stability at low temperatures. Kinetic analysis was limited to the range of 350 -390 ° C finding that, the apparent activation energy is not significantly different for bimetallic catalysts, and for the Pt monometallic catalyst it is slightly less and the catalytic combustion of methane in Pt-Fe catalysts is close to the first order for methane and negative zero order for oxygen. Finally, the synergy of the bimetallic systems seemed to be dominated by the platinum dispersion.

This work allowed to develop an impregnation method following a route guided by the characterization of the materials and a unit line of processes through which it was possible to produce Pt-Fe catalysts supported on silica, the results achieved evidenced the possibility of obtaining favorable catalytic results in the combustion of methane with low platinum loads, which would reduce its cost and favor the stability of the catalysts in reaction.

Bibliographic references

1. Nalwa H. Handbook of Surfaces and Interfaces of Materials. 2001.

2. Mehrabadi BAT, Eskandari S, Khan U, White RD, Regalbuto JR. A Review of Preparation Methods for Supported Metal Catalysts. Adv Catal. 2017;61.

3. Regalbuto JR. A scientific method to prepare supported metal catalysts. Surf Nanomolecular Catal. 2006;161–94.

4. Satterfield C. Heterogeneous catalysis in industrial practice. 1996. 88–93 p.

5. Zhu X, Cho H, Pasupong M, Regalbuto JR. Charge-Enhanced Dry Impregnation: A Simple Way to Improve the Preparation of Supported Metal Catalysts. ACS Catal [Internet]. 2013 Apr 5;3(4):625–30. Available from: https://pubs.acs.org/doi/10.1021/cs3008347

6. Spieker WA, Regalbuto JR. Afundamental model of platinum impregnation onto alumina. Chem Eng Sci. 2001;56:3491–3504.

7. Falco L, Peluso M, Sambeth J, Thomas H. Recovery of manganese oxides from spent alkaline and zinc-carbon batteries. An application as catalysts for VOCs elimination. Waste Manag. 2013;33(2013):1483–90.

8. Kumar M, Rattan G, Prasad R. Catalytic Abatement of Methane Emission from CNG Vehicles: An Overview. Can Chem Trans. 2015;3(2015):381–409.

9. He L, Fan Y, Bellettre J, Yue J, Luo L. A review on catalytic methane combustion at low temperatures: Catalysts, mechanisms, reaction conditions and reactor designs. Renew Sustain Energy Rev [Internet]. 2020 Mar;119:109589. Available from: https://linkinghub.elsevier.com/retrieve/pii/S136403211930797X

10. Eman EA. GAS FLARING IN INDUSTRY: AN OVERVIEW. Pet Coal J. 2015;57(2015):532–55.

11. Elvidge CD, Zhizhin M, Baugh K, Hsu F-C, Ghosh T. Methods for Global Survey of

Natural Gas Flaring from Visible Infrared Imaging Radiometer Suite Data. energies. 2016;9(14).

12. Speight JG, Özüm B. Petroleum refinery processes. 2001. 35 p.

13. UNIONgas. Chemical Composition of Natural Gas. https://www.uniongas.com/about-us/about-natural-gas/chemical-composition-of-natural-gas. 2017.

14. Jiang X, Mira D, Cluff D. The combustion mitigation of methane as an on-CO2 greenhouse gas. Prog Energy Combust Sci. 2018;66:176–99.

15. Kim S jin, Park S in, Lee JC, Seo JK, Kim B ju, Ha Y chul. Experimental study of the reduction of high temperatures and radiation using heat shields associated with flare towers of offshore oil and gas platforms. Ships offshore Struct. 2014;9(5).

16. Lee JH, Trimm DM. Catalytic combustion of methane. El Sevier. 1995;42:339–59.

17. Aguilera DA. Catalizadores de Mn-Cu y Mn-Co sintetizados a partir de hidrotalcitas y su empleo en la oxidación de COVs. 2010.

18. Schneider SH. The Greenhouse Effect: Science and Policy. Ciesin. 1989;243:771–81.

19. Denver Gold Group. Precious Metal Prices and Charts. https://www.denvergold.org/precious-metal-prices-charts/. 2021.

20. Chen J, Arandiyan H, Gao X, Li J. Recent Advances in Catalysts for Methane Combustion. Catal Surv Asia. 2015;19:140–71.

21. Roth D, Gelin P, Tena E, Primet M. Combustion of methane at low temperature over Pd and Pt catalysts supported on Al2O3, SnO2 and Al2O3-grafted SnO2. Top Catal. 2001;16/17:1–4.

22. Cho H-R, Regalbuto JR. The rational synthesis of Pt-Pd bimetallic catalysts by electrostatic adsorption. Catal Today. 2015;246:143–53.

23. Qu P, Wang S, Hu W, Wu Y, Chen J, Zhang G, et al. A novel strategy to design PtPd bimetallic catalysts for efficient methane combustion. Catal Commun [Internet]. 2020 Feb;135:105900. Available from: https://linkinghub.elsevier.com/retrieve/pii/S1566736719303619

24. Drozdov VA, Tsyrulnikov PG, Popovskii V V., Bulgakov NN, Moroz EM, Galeev TG. Comparative study of the activity of Al−Pd and Al−Pt catalysts in deep oxidation of hydrocarbons. React Kinet Catal Lett [Internet]. 1985 Sep;27(2):425–7. Available from: http://link.springer.com/10.1007/BF02070487

25. Burch R, Loader PK. Investigation of Pt/Al2O3 and Pd/Al2O3 catalysts for the combustion of methane at low concentrations. Appl Catal B Environ [Internet]. 1994 Dec;5(1–2):149–64. Available from: https://linkinghub.elsevier.com/retrieve/pii/0926337394000379

26. Statista. Iron oxide price in the United States from 2013 to 2018 (in U.S. dollars per kilogram)*. https://www.statista.com/statistics/881746/average-us-iron-oxide-price/. 2018.

27. Liu Q, Zhang Z. Platinum single-atom catalysts: a comparative review towards effective characterization. Catal Sci Technol [Internet]. 2019;9(18):4821–34. Available from: http://xlink.rsc.org/?DOI=C9CY01028A

28. Liu G, Walsh AG, Zhang P. Synergism of Iron and Platinum Species for Low-Temperature CO Oxidation: From Two-Dimensional Surface to Nanoparticle and Single-Atom Catalysts. J Phys Chem Lett [Internet]. 2020 Mar 19;11(6):2219–29. Available from: https://pubs.acs.org/doi/10.1021/acs.jpclett.9b03311

29. Bian C, Zhang C, Pan S, Fang Chen, Weiping Zhang, Xiangju Meng, et al. Generalized high-temperature synthesis of zeolite catalysts with unpredictably high space-time yields (STYs). J Mater Chem A. 2017;5:2613–8.

30. Seeburg D, Liu D, Radnik J, Atia H, Pohl M-M, Schneider M, et al. Structural Changes of Highly Active Pd/MeOx (Me = Fe, Co, Ni) during Catalytic Methane Combustion. Catalysts. 2018;8(2):42.

31. Kamal MS, Razzak SA, Hossain MM. Catalytic oxidation of volatile organic compounds (VOCs) — a review. Atmos Environ. 2016;

32. Sirijaruphan A, Goodwin Jr. JG, Rice RW, Wei D, Butcher KR, Roberts GW, et al. Effect of metal foam supports on the selective oxidation of CO on Fe-promoted Pt/γ-Al2O3. Appl Catal A Gen [Internet]. 2005 Mar;281(1–2):11–8. Available from: https://linkinghub.elsevier.com/retrieve/pii/S0926860X0400910X

33. Siani A, Captain B, Alexeev OS, Stafyla E, Hungria AB, Midgley PA, et al. Improved CO Oxidation Activity in the Presence and Absence of Hydrogen over Cluster-Derived PtFe/SiO 2 Catalysts. Langmuir [Internet]. 2006 May;22(11):5160–7. Available from: https://pubs.acs.org/doi/10.1021/la053476a

34. Chai Z, Zhang C, Wang H, Bi X, Bai P, Wang X. Increased interface effects of Pt Fe alloy/CeO2/C with Pt Fe selective loading on CeO2 for superior performance in direct methanol fuel cell. Int J Hydrogen Energy [Internet]. 2019 Feb;44(10):4794–808. Available from: https://linkinghub.elsevier.com/retrieve/pii/S036031991930059X

35. Rodriguez JR, Félix RM, Reynoso EA, Gochi-Ponce Y, Gómez YV, Moyado SF, et al. Synthesis of Pt and Pt-Fe nanoparticles supported on MWCNTs used as electrocatalysts in the methanol oxidation reaction. J Energy Chem [Internet]. 2014 Jul;23(4):483–90. Available from: https://linkinghub.elsevier.com/retrieve/pii/S2095495614601753

36. Yuan W, Scott K, Cheng H. Fabrication and evaluation of Pt–Fe alloys as methanol tolerant cathode materials for direct methanol fuel cells. J Power Sources [Internet]. 2006 Dec;163(1):323–9. Available from: https://linkinghub.elsevier.com/retrieve/pii/S0378775306018325

37. Mahmood T, Saddique MT, Naeem A, Westerhoff P, Mustafa S, Alum A. Comparison of Different Methods for the Point of Zero Charge Determination of NiO. Am Chem Soc. 2011;50:10017–10023.

38. Brunauer S, Emmett P., Teller E. Adsorption of gases in multimolecular layers.

JACS. 1938;60(2):309–19.

39. Rouquerol J, Rouquerol F, Sing K. Adsorption by Powders and Porous Solids. 1998. 210 p.

40. Thommes M, Kaneko K, Neimark A, Olivier J, Rodriguez-Reinoso F, Rouquerol J, et al. Physisorption of gases, with special reference to the evaluation of surface area and pore size distribution (IUPAC Technical Report). 2015.

41. Westerman DWB, Ruffio IE, Wainwright MS, Foster NR. Chemical analysis of vanadium pentoxide catalysts. Anal Chim Acta. 1980;117:285–91.

42. Hiden Analytical. Relative Sensitivity - RS Measurements of Gases [Internet]. 2020. Available from: http://www.hiden.de/wp-content/uploads/pdf/RS_Measurement_of_Gases_-_Hiden_Analytical_App_Note_282.pdf

43. Wojdyr M. Fityk: a general-purpose peak fitting program. Appl Crystallogr. 2010;43(5):1126–1128.

44. Reynoso AJ, Ayastuy JL, Iriarte U, Miguel Ángel GO. Bimetallic Pt-Co Catalysts for the Liquid-Phase WGS. Catalysts. 2020;10:830.

45. Fadoni M, L.Lucarelli. Temperature programmed desorption , reduction , oxidation and flow chemisorption for the characterisation of heterogeneous catalysts . Theoretical aspects , instrumentation and applications. 2006;

46. Torrente-Murciano L. The importance of particle-support interaction on particle size determination by gas chemisorption. J Nanopart Res. 2016;18(87).

47. Paolucci C, Parekh AA, Khurana I, Iorio JR Di, Li H, Albarracin J, et al. Catalysis in a Cage: Condition-Dependent Speciation and Dynamics of Exchanged Cu Cations in SSZ-13 Zeolites. J Am Chem Soc. 2016;

48. Massaldi HA, Maymó JA. Error in Handling Finite Conversion Reactor Data by the Diff erentiai Method. J Catal. 1969;14:61–8.

49. Qi W, Ran J, Wang R, Du X, Shi J, Niu J, et al. Kinetics Consequences of Methane Combustion on Pd, Pt and Pd-Pt Catalysts. RSC Adv. 2016;6.

50. Sandoval S, Morales EM, Baldovino V, Castillo C. Kinetic assessment of the dry reforming of methane over a solid solution Ni–La oxide catalyst. 2021;

51. Sandoval VS, Peña JA. Diseño, construcción y puesta en marcha de un sistema automatizado de reactores a escala laboratorio, acoplado a cromatografía de gases para reacciones de oxidación y reformado. 2017.

52. Brown A. A step-by-step guide to non-linear regression analysis of experimental data using a Microsoft Excel spreadsheet. Comput Methods Programs Biomed. 2001;65:191–200.

53. Montgomery DC, Runger GC. Applied Statistics and Probability for Engineers. 349 p.

54. L. T. Zhuravlev. Concentration of hydroxyl groups on the surface of amorphous silicas. Langmuir. 1987;3:316–8.

55. Colvin CB. Kinetics of ligand substitution for platinum(II) complexes. 1962.

56. MILLER J. A fundamental study of platinum tetraammine impregnation of silica2. The effect of method of preparation, loading, and calcination temperature on (reduced) particle size. J Catal [Internet]. 2004 Jul;225(1):203–12. Available from: https://linkinghub.elsevier.com/retrieve/pii/S0021951704001885

57. Pansuriya PB, Patel MN. Iron(III) complexes: Preparation, characterization, antibacterial activity and DNA-binding. J Enzyme Inhib Med Chem [Internet]. 2008 Jan 1;23(2):230–9. Available from: https://www.tandfonline.com/doi/full/10.1080/14756360701474657

58. Broennum B, Johansen HS, Skibsted LH. Ammine ligand exchange in tetraammineplatinum(II) in aqueous solution. Inorg Chem [Internet]. 1992 Jul 1;31(14):3023–5. Available from: https://pubs.acs.org/doi/abs/10.1021/ic00040a008

59. Radivojević D, Seshan K, Lefferts L. Preparation of well-dispersed Pt/SiO2 catalysts using low-temperature treatments. Appl Catal A Gen [Internet]. 2006 Feb;301(1):51–8. Available from: https://linkinghub.elsevier.com/retrieve/pii/S0926860X05008756

60. Masashi Kotobuki, Akiko Watanabe, Hiroyuki Uchida, Yamashita H, Watanabe M. High catalytic performance of Pt-Fe alloy nanoparticles supported in mordenite pores for preferential CO oxidation in H2-rich gas. Appl Catal A Gen. 2006;307:275–283.

61. Navas Cárdenas C, Enito N, Wolf EE, Gracia F. Effect of Pt-MOx (M=Fe, Co) interaction on the preferential oxidation of CO over Pt/MOx/TiO2 catalysts prepared by selective electrostatic adsorption. Appl Catal A Gen. 2019;576:11–19.

62. Isaifan RJ, Ntais S, Baranova EA. Particle size effect on catalytic activity of carbon-supported Pt nanoparticles for complete ethylene oxidation. Appl Catal A Gen [Internet]. 2013 Aug;464–465:87–94. Available from: https://linkinghub.elsevier.com/retrieve/pii/S0926860X13003086

63. Lu Y, Du S, Steinberger-Wilckens R. Temperature-controlled growth of single-crystal Pt nanowire arrays for high performance catalyst electrodes in polymer electrolyte fuel cells. Appl Catal B Environ [Internet]. 2015 Mar;164:389–95. Available from: https://linkinghub.elsevier.com/retrieve/pii/S0926337314005748

64. Johansson T, Pakhare D, Haynes D, Abdelsayed V, Dushyant Shekhawat JS. Characterization of LaRhO3 perovskites for dry (CO2) reforming of methane (DRM). Chem Pap. 68(9):1240–1247.

65. Dreyer JA., Grossmann HK, Chen J, Grieb T, Gong B. Preferential oxidation of carbon monoxide over Pt–FeOx/CeO2 synthesized by two-nozzle flame spray pyrolysis. J Catal. 2015;329:248–261.

66. Arnoldy P. Temperature-Programmed Reduction of A1203-, Si02-, and Carbon-Supported Re207 Catalysts. J Catal. 1985;93:231–45.

67. Einaga H, Urahama N, Tou A, Teraoka Y. CO Oxidation Over TiO2-Supported Pt–Fe Catalysts Prepared by Coimpregnation Methods. Catal Lett. 2014;

68. An N, Qiushi Yu, Liu G, Li S, Jia M, Zhang W. Complete oxidation of formaldehyde at ambient temperature over supported Pt/Fe2O3 catalysts prepared by colloid-deposition method. J Hazard Mater. 2011;28(2–3):1392–7.

69. Rodriguez J. EFECTO DE LA PROPORCIÓN ENTRE PLATINO Y RENIO EN EL ESTADO QUÍMICO SUPERFICIAL Y EL DESEMPEÑO CATALÍTICO DE Pt-Re/□-Al2O3 EN PROCESOS DE REFORMADO CON BÚSQUEDA DE UN MENOR CONSUMO ENERGÉTICO. 2018.

70. Solange N, Eon J-G, Schmal M. Dispersion of Platinum on Alumina-Grafted Titanium Oxide. J Catal. 1999;183:6–13.

71. Rui Z, Chen L, Chen H, Ji H. Strong Metal-Support Interaction in Pt/TiO 2 Induced by Mild HCHO and NaBH 4 Solution Reduction and Its Effect on Catalytic Toluene Combustion. Ind Eng Chem Res [Internet]. 2014 Oct 15;53(41):15879–88. Available from: https://pubs.acs.org/doi/10.1021/ie5029107

72. SinhaRay S, Gusain R, Kumar N. Chapter four - Adsorption in the context of water purification. In: Carbon Nanomaterial-Based Adsorbents for Water Purification. 2020. p. 67–100.

73. Kota AS, Dadi RK, Luss D, Balakotaiah V. Analysis of light-off during oxidation of reactant mixtures on Pt/Al2O3 using micro-kinetic models. Chem Eng Sci. 2017;

74. Carlsson P-A, Skoglundh M. Low-temperature oxidation of carbon monoxide and methane over alumina and ceria supported platinum catalysts. Appl Catal B Enviromental. 2011;101(3–4):669–75.

75. Carlsson P-A, Österlund L, Thormählen P, Palmqvist A, Fridella E, Jansson J, et al. A transient in situ FTIR and XANES study of CO oxidation over Pt/Al2O3 catalysts. J Catal. 2004;226(2):422–34.

76. Casapu M, Fischer A, Gänzler AM, Popescu R, Crone M, Gerthsen D, et al. Origin

of the Normal and Inverse Hysteresis Behavior during CO Oxidation over Pt/Al2O3. ACS Catal. 2017;7(1):343–355.

77. Kinnunen NM, Hirvi JT, Suvanto M, Pakkanen TA. Methane combustion activity of Pd–PdOx–Pt/Al2O3 catalyst: The role of platinum promoter. J Mol Catal A Chem [Internet]. 2012 Apr;356:20–8. Available from: https://linkinghub.elsevier.com/retrieve/pii/S1381116911005401

78. Neuberg S, Pennemann H, Shanmugam V, Zapf R, Kolb G. Promoting effect of Rh on the activity and stability of Pt-based methane combustion catalyst in microreactors. Catal Commun [Internet]. 2021 Jan;149:106202. Available from: https://linkinghub.elsevier.com/retrieve/pii/S1566736720302788

79. Yao Y-FY. Oxidation of Alkanes over Noble Metal Catalysts. Ind Eng Chem Prod Res Dev [Internet]. 1980 Sep 1;19(3):293–8. Available from: https://pubs.acs.org/doi/abs/10.1021/i360075a003

80. Abbasi R, Wu L, Wanke SE, Hayes RE. Kinetics of methane combustion over Pt and Pt–Pd catalysts. Chem Eng Res Des [Internet]. 2012 Nov;90(11):1930–42. Available from: https://linkinghub.elsevier.com/retrieve/pii/S0263876212001141

81. Paranjpe R, Suresh AK, Aghalayam P. Understanding Pt–Rh Synergy in a Three-Way Catalytic Converter. Int J Chem React Eng. 2013;11(1):1–8.

82. Precht R, Stolz S, Mankel E, Mayer T, Jaegermann W, Hausbrand R. Investigation of sodium insertion into tetracyanoquinodimethane (TCNQ): results for a TCNQ thin film obtained by a surface science approach. Phys Chem Chem Phys [Internet]. 2016;18(4):3056–64. Available from: http://xlink.rsc.org/?DOI=C5CP06659J

83. Savintsev AP, Gavasheli YO, Kalazhokov ZK, Kalazhokov KK. X-ray photoelectron spectroscopy studies of the sodium chloride surface after laser exposure. J Phys Conf Ser [Internet]. 2016 Nov;774:012118. Available from: https://iopscience.iop.org/article/10.1088/1742-6596/774/1/012118

84. Cloarec J-P, Chevalier C, Genest J, Beauvais J, Chamas H, Chevolot Y, et al. pH

driven addressing of silicon nanowires onto Si 3 N 4 /SiO 2 micro-patterned surfaces. Nanotechnology [Internet]. 2016 Jul 22;27(29):295602. Available from: https://iopscience.iop.org/article/10.1088/0957-4484/27/29/295602

85. Phanichphant S, Nakaruk A, Channei D. Photocatalytic activity of the binary composite CeO2/SiO2 for degradation of dye. Appl Surf Sci [Internet]. 2016 Nov;387:214–20. Available from: https://linkinghub.elsevier.com/retrieve/pii/S0169433216312995

86. DeFarias R., Airoldi C. Thermogravimetry as a reliable tool to estimate the density of silanols on a silice gel surface. J Therm Anal. 1998;53:751–6.

87. Liu X., Thomanson J., Jones F. The concentration of hydroxyl Groups on glass surfaces and their effect on the structure of silane deposits. Silanes and Other Coupling Agents-. 2009;5:25–8.

88. Karakaya C, Deutschmann O. A simple method for CO chemisorption studies under continuous flow: Adsorption and desorption behavior of Pt/Al2O3 catalysts. Appl Catal A Gen [Internet]. 2012 Nov;445–446:221–30. Available from: https://linkinghub.elsevier.com/retrieve/pii/S0926860X12005443

89. Kiakalaieh AT, Amin NAS. Theoretical and experimental evaluation of mass transfer limitation in gas phase dehydration of glycerol to acrolein over supported HSiW catalyst. J Taiwan Inst Chem Eng. 2016;59:11–17.

90. Xiao Y, Varma A. Kinetics of Guaiacol Deoxygenation Using Methane over Pt-Bi Catalyst. React Chem Eng. 2016;2(1):36–43.

Appendix

Appendix A. *Support characterization*

The binding energy of approximately 1070.0[82,83] indicates the presence of sodium as a contaminant in the SiO_2 support (Figure S1a), while after washing the signal for Na1s was not observed, guaranteeing the total removal of sodium (Figure S1b).

Figure S1.

XPS spectra of Na-SiO_2. a) Before removing sodium b) After washing with HNO_3

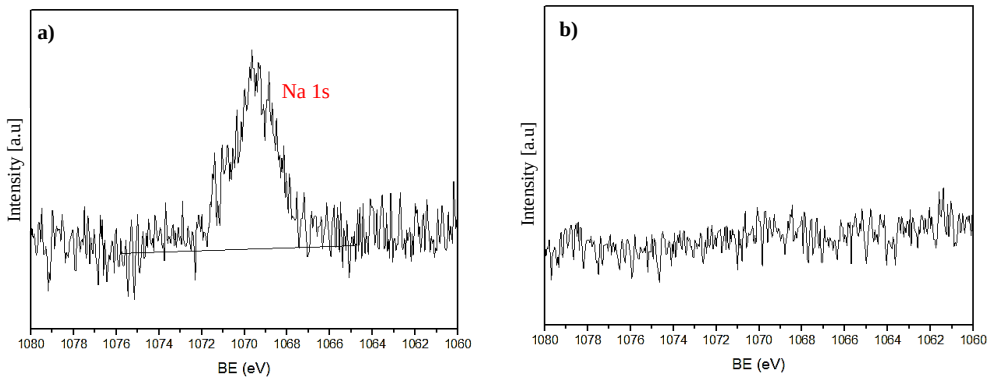

Figure S2 shows the characteristics adsorption-desorption isotherm of N_2 for the support (SiO_2).

Figure S2.

N_2 adsorption-desorption isotherm

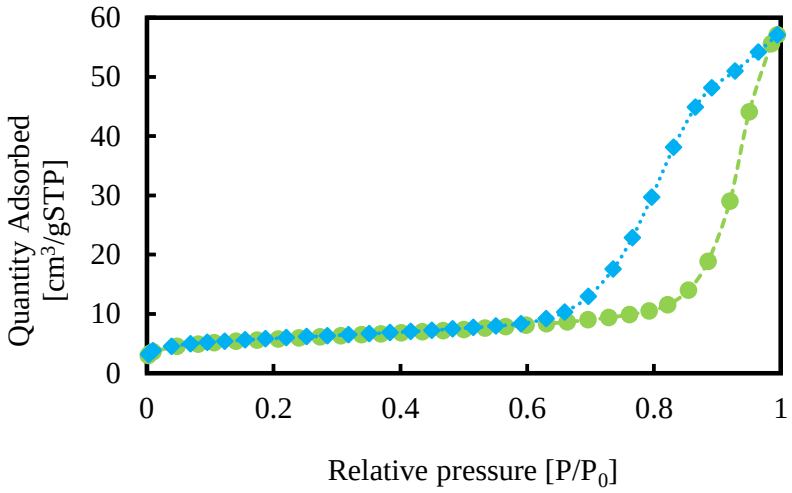

For the analysis of the porosity of the support 6 replicas of the test were carried out, the data is presented in Table S1.

Table S1.

Results of the BET Area and the constant C_{BET} for the support

Sample	BET area [m^2/g]	C_{BET}
SiO_2-1	19.30	139.82
SiO_2-2	19.27	136.42
SiO_2-3	18.99	139.76
SiO_2-4	18.97	137.92
SiO_2-5	18.97	137.92
SiO_2-6	20.31	142.78
Average	19.30	
Standard deviation	0.515	

The value of PZC was estimated from the intercepts of the curve with the x axis, for this support the expected value of PZC is around 3 [84,85], doubling the experiment allowed to find a deviation of 0.1 in the reported value (Figure S3).

Figure S3.

Point of Zero Charge for SiO_2. The experiment is shown in duplicate

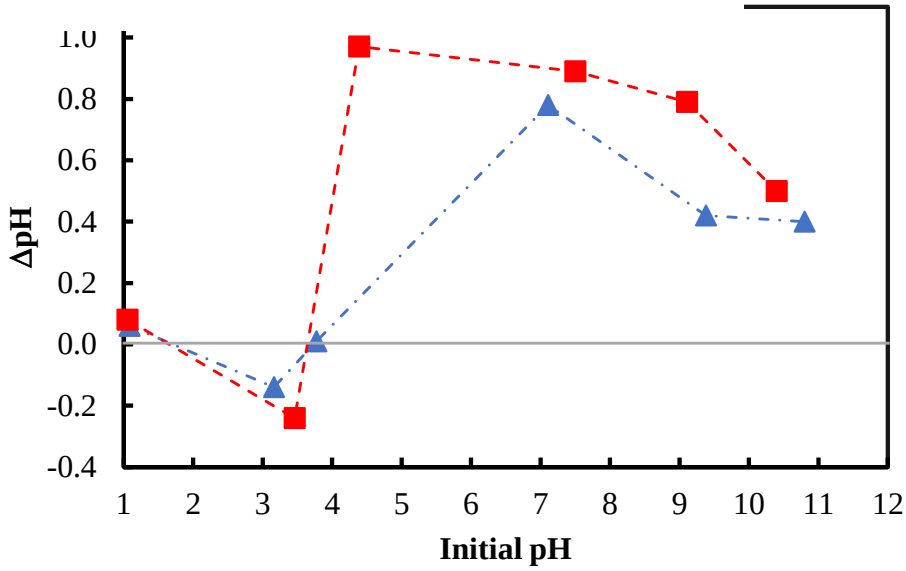

In Figure S4 two changes are observed in the function derived from weight with respect to temperature, the first corresponds to the H_2O molecules that are physisorbed in the material, while the second change, of less intensity, corresponds to the molecules of water that are formed after the following reaction[86]:

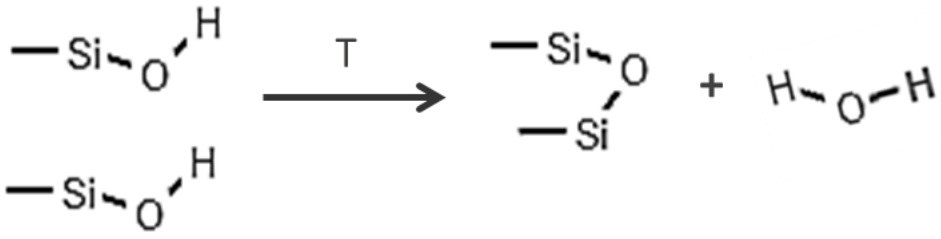

Therefore, it could be considered that each water molecule formed comes from two silanol groups present on the support.

Figure S 4.

TGA and DTGA for SiO_2. under a static N_2 atmosphere.

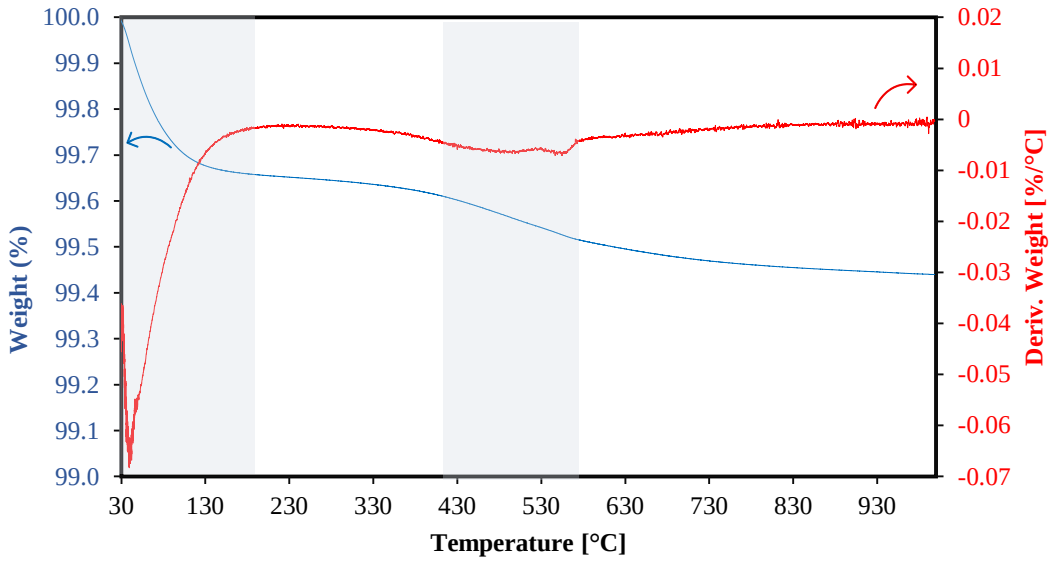

The change in the derivative occurred from 410.87 to 554.04 with a mass loss of 0.1613%. Table S1 summarizes the data required for the calculation of the OH density.

Table S2.

Data required for the calculation of the OH density

Initial mass TGA [g]	18.33
Temperature range [°C]	410.87 - 554.04
Mass loss [%]	0.1643%
Support area (SiO_2) [nm^2/g]	1.93E+19
Avogadro's number	6.022E+23
MW Pt [g/mol]	195.08
MW Fe [g/mol]	55.845
MW H_2O[g/mol]	18.015

The mathematical procedure proposed by DeFarias and Airoldi[86] is shown below:

$$18.33g * \frac{0.1643\%}{100} = 0.03012\ g \quad \text{mass of } H_2O \text{ lost during heating}$$

$$\frac{0.03012\ g}{18.015\frac{g}{mol}} * 6.022 \cdot 10^{23}\ \frac{molecules\ H_2O}{mol} = 1.007 \cdot 10^{21}\ molecules\ of\ H_2O$$

$$\frac{1.007 \cdot 10^{21}\ H_2O\ molecules * 2\ \frac{OH\ molecules}{H_2O\ molecules}}{1.93 \cdot 10^{19}\frac{nm^2}{g} * 18.33\ g} = 5.697\ \frac{OH}{nm^2}$$

The density of silanol groups is 5.697 OH/nm^2. The calculations made will be used to calculate the maximum percentage of metal that will be impregnated to obtain a monolayer in 5g of support.

$$5.697\frac{OH}{nm^2} * 1.93 \cdot 10^{19}\frac{nm^2}{g} * 5\ g = 5.50 \cdot 10^{20}\ OH$$

$$\frac{2.75 \cdot 10^{20}\ Pt\ molecules}{6.022 \cdot 10^{23}\frac{molecules}{mol}} = 0.00046\ mol\ Pt$$

$$0.00046\ mol\ Pt * 195.08\ \frac{g}{mol} = 0.0890\ g\ Pt$$

$$\%wPt = \frac{0.0890}{0.0890 + 5} = 1.75\%Pt$$

$$\frac{2.75 \cdot 10^{20}\ Fe\ molecules}{6.022 \cdot 10^{23}\ \frac{molecules}{mol}} = 0.00046\ mol\ Fe$$

$$0.00046\ mol\ Fe * 55.845\ \frac{g}{mol} = 0.0255\ g\ Fe$$

$$\%wFe = \frac{0.0255}{0.0255 + 5} = 0.51\%Fe$$

With these values, the weight percentages for the catalysts to be prepared (Table S2) were calculated, maintaining a load of 460 mmol of metals for 5g of support.

Table S3. Weight percent for the catalysts

Mole fraction of Pt	1	0.75	0.5	0.25	0
Pt	1.75%	1.31%	0.88%	0.44%	0.00%
Fe	0.00%	0.13%	0.25%	0.38%	0.50%

On the other hand, variations in pH in silica promote the following reactions:

$$Si - OH_2^+ \rightarrow Si - OH + H^+ \qquad Si - OH \rightarrow Si - O^- + H^+$$

$$K_1 = \frac{[SiOH][H^+]}{[SiOH_2^+]} \qquad K_2 = \frac{[SiO^-][H^+]}{[SiOH]}$$

So, it would be expected to have two equivalent points, one between (Si-OH_2^+ and Si-OH) and the second between (Si-OH and Si-O^-). To find the inflection point that would mark the equivalence point, the criterion of the second derivative is used in the titration curve (Figure S5).

Figure S5.

Titration curve for SiO_2. A polynomial degree 5 was fitted, obtaining a value of R^2 of 0.998.

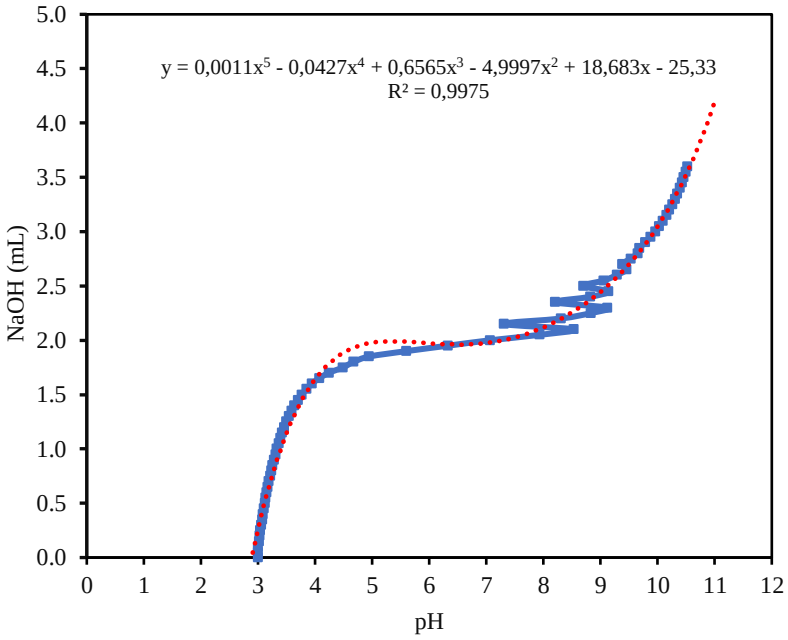

$$f(x) = 0.0011x^5 - 0.0427x^4 + 0.6565x^3 - 4.9997x^2 + 18.683x - 25.332$$

$$f''(x) = 0.014x^3 - 0.3264x^2 + 2.7126x - 7.4254 \quad f''(x) = 0$$

$$0 = 0.014x^3 - 0.3264x^2 + 2.7126x - 7.4254$$

x=5.63

Thus, pk_2 = 5.63 y K_2= $2.34 \cdot 10^{-6}$. At PZC, the surface density of positive charges is equal to the density of negative charges, for which it is possible to deduce the following equations:

$$K_1 * K_2 = [H^+]^2 \qquad PZC = pH = -\frac{1}{2}\log(K_1 * K_2)$$

$$3.5 = -\frac{1}{2}\log\left(K_1 * 2.34 \cdot 10^{-6}\right)$$

K_1= 0.0436 pk_1= 1.37

Knowing the equilibrium points between the species it is possible to make the diagram of the molar fraction with respect to the pH (Figure S6), finding similar results in the literature[87].

Figure S6 shows that due to the acidic characteristics of silica, the surface will never be fully positively charged, on the other hand, a pH greater than 8 will provide a surface full of negative groups.

Figure S6.

Species distribution diagram with respect to pH

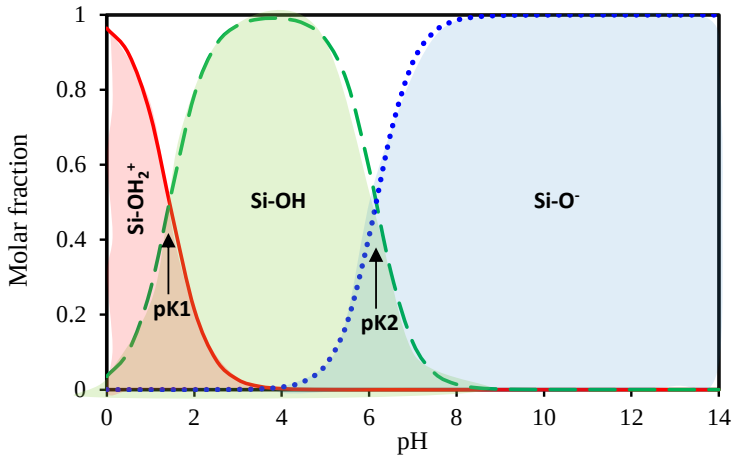

Appendix B. Thermal treatment

Figure S7 shows MS response obtained for H_2O and CO_2 during the H_2-TPR tests for the prepared catalysts. In all cases, the elimination of water and carbon dioxide was observed in the range of 400 -600 °C.

Figure S7.

MS response for H_2O and CO_2 during H_2-TPR. Before analysis catalyst were calcined at 300°C for 3h in Ar atmosphere.

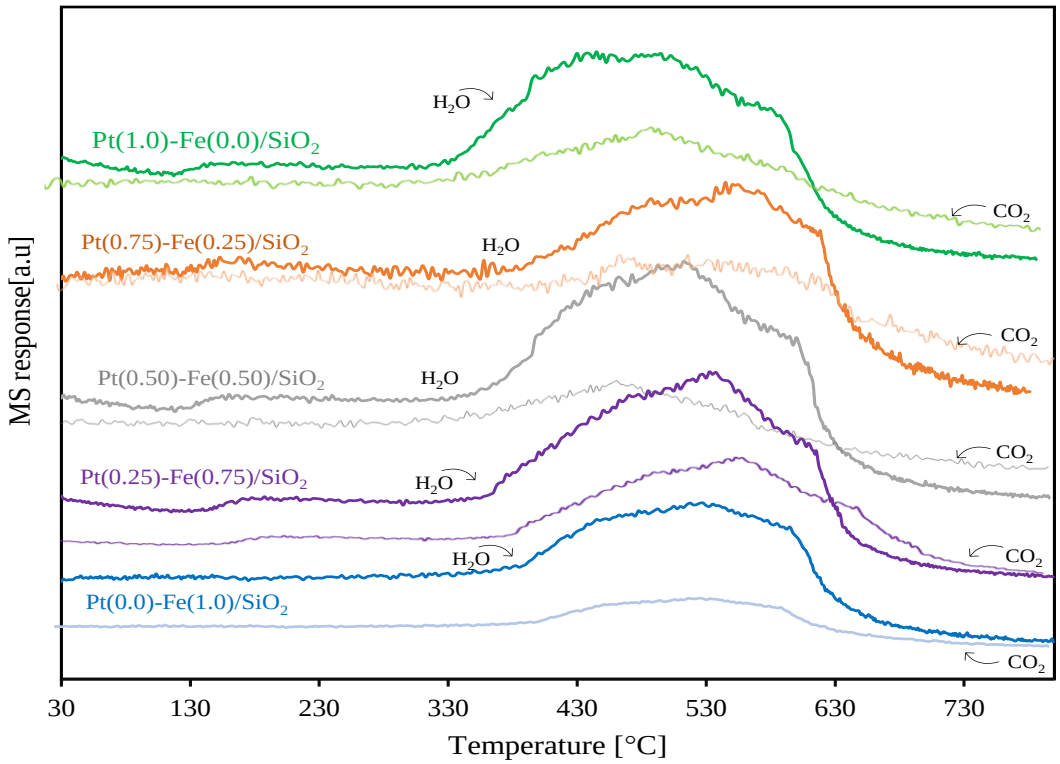

Figure S8 shows the reduction profiles for the catalysts during 90 min, additionally, the peak deconvolution was performed, the analysis for this situation is the same as that presented in the main text.

Figure S8.

Time trial for complete reduction at low temperature.

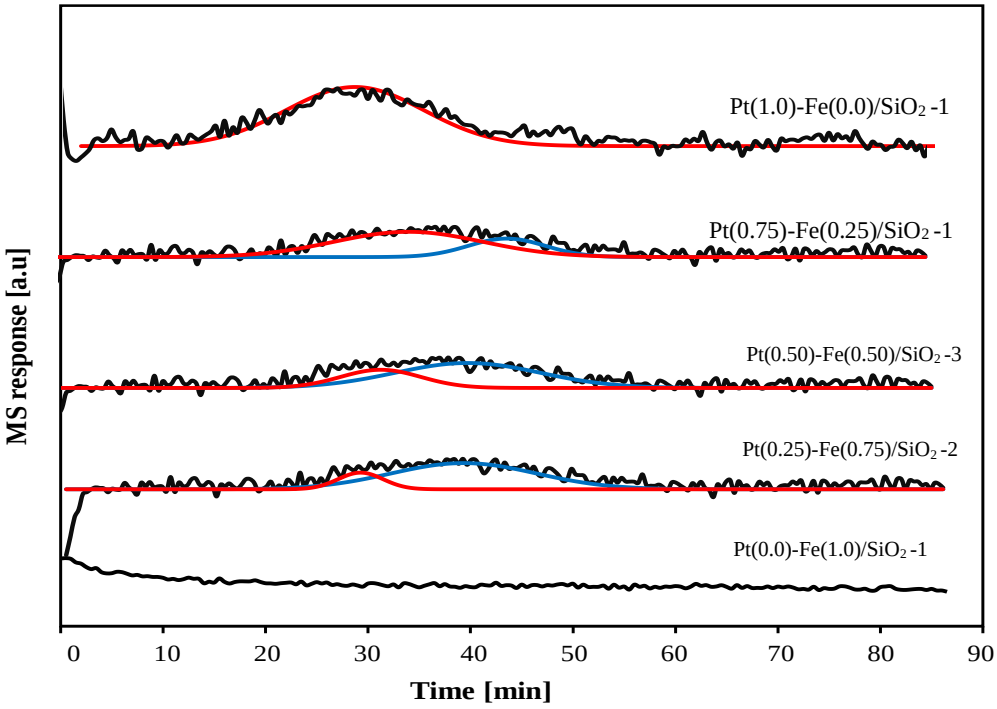

Note: Temperature was kept constant at 200 ° C. Before analysis catalyst were calcined at 300°C for 3h in Ar atmosphere. Catalysts were randomly selected for testing.

Appendix C. Characterization

N_2 physisorption. Figure S9 shows the adsorption-desorption isotherms of N_2 for the catalysts and the support, their shape did not change despite impregnation and subsequent heat treatment. Individual results are shown in Table S4.

Figure S9.

Adsorption- desorption N_2 isotherms. a) Fresh catalysts; b) Calcined catalysts. c) Reduced catalysts. Catalysts were randomly selected for testing.

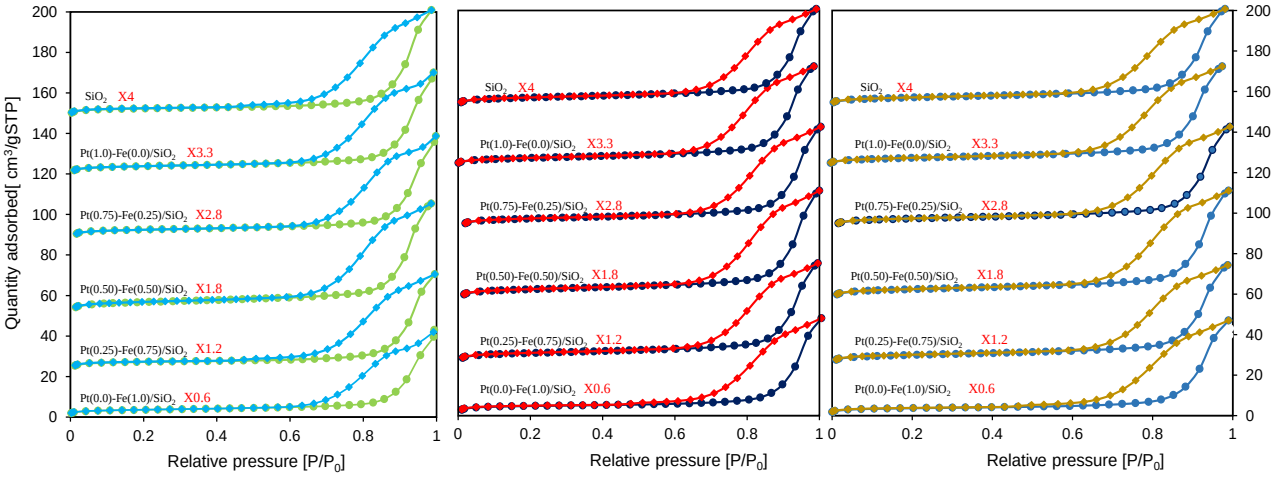

Table S4.

Results for BET area of the catalysts, for the test the replicas were randomly selected.

		Replica				
		1	2	3	Average	Standard deviation
Fresh	Pt(0.0)-Fe(1.0)/SiO_2	14.9	-	15.2	15.1	0.21
	Pt(0.25)-Fe(0.75)/SiO_2	15.9	16.9	-	16.4	0.71
	Pt(0.50)-Fe(0.50)/SiO_2	-	15.8	17.9	16.9	1.48
	Pt(0.75)-Fe(0.25)/SiO_2	14.9	-	15.4	15.1	0.37
	Pt(1.0)-Fe(0.0)/SiO_2	-	14.9	15.3	15.1	0.28
Calcined	Pt(0.0)-Fe(1.0)/SiO_2	15.2	15.0	15.0	15.1	0.12
	Pt(0.25)-Fe(0.75)/SiO_2	14.9	-	15.0	15.0	0.07
	Pt(0.50)-Fe(0.50)/SiO_2	15.8	16.3	-	16.1	0.35
	Pt(0.75)-Fe(0.25)/SiO_2	-	14.9	14.7	14.8	0.14
	Pt(1.0)-Fe(0.0)/SiO_2	14.3	-	14.8	14.6	0.35
Reduced	Pt(0.0)-Fe(1.0)/SiO_2	15.2	15.4	-	15.3	0.14
	Pt(0.25)-Fe(0.75)/SiO_2	14.8	-	14.8	14.8	0.00
	Pt(0.50)-Fe(0.50)/SiO_2	16.1	-	16.6	16.4	0.35
	Pt(0.75)-Fe(0.25)/SiO_2	14.1	14.9	15.3	14.8	0.60
	Pt(1.0)-Fe(0.0)/SiO_2	-	14.3	14.9	14.6	0.42

CO and O_2 chemisorption. The first step is the determination of the possible consumption of CO by iron particles and O_2 by Pt particles (Figure S10).

Figure S10.
Chemisorption of CO and O_2

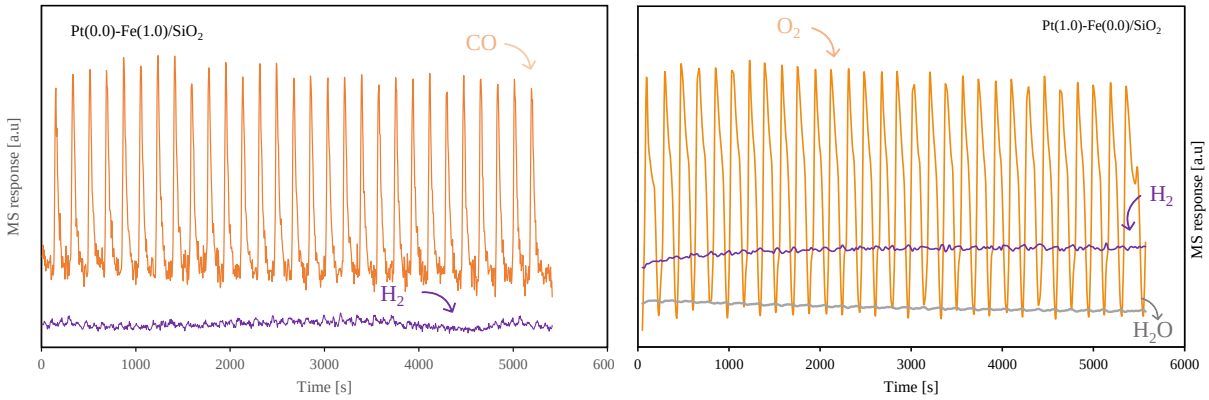

Note: Chemisorption of CO for the iron monometallic catalyst Pt(0.0)-Fe(1.0)/SiO_2. O_2 chemisorption for the platinum monometallic catalyst Pt(1.0)-Fe(0.0)/ SiO_2. Before analysis catalyst were calcined at 300°C for 3h in Ar atmosphere and reduced in H2 at 200° C.

The individual results for the three replicates are shown in Table S5.

Table S5.

PtFe catalyst dispersions.

CO Chemisorption - Pt dispersion results						
Sample	1	2	3	Average	Standard deviation	Standard error*
Pt(0.0)-Fe(1.0)/SiO_2	-	-	-	-	-	-
Pt(0.25)-Fe(0.75)/SiO_2	74.27	82.3	80.4	79.0	4.197	2.423
Pt(0.50)-Fe(0.50)/SiO_2	54.2	66.0	59.9	60.0	5.901	3.407
Pt(0.75)-Fe(0.25)/SiO_2	20.96	17.3	18.45	18.9	1.872	1.081
Pt(1.0)-Fe(0.0)/SiO_2	13.99	13.2	12.3	13.2	0.846	0.488
O_2 Chemisorption - Fe dispersion results						
Sample	1	2	3	Average		Standard error*
Pt(0.0)-Fe(1.0)/SiO_2	22.1	19.45	18.4	20.0	1.907	1.101
Pt(0.25)-Fe(0.75)/SiO_2	53.15	51.2	50.2	51.5	1.500	0.866
Pt(0.50)-Fe(0.50)/SiO_2	80.79	75.2	71.5	75.8	4.677	2.700
Pt(0.75)-Fe(0.25)/SiO_2	94.17	90.4	87.5	90.7	3.344	1.931
Pt(1.0)-Fe(0.0)/SiO_2	-	-	-	-	-	-

Note: The standard error corresponds to the standard deviation divided by the root of the amount of data. Before analysis catalyst were calcined at 300°C for 3h in Ar atmosphere and reduced in H_2 at 200° C.

The response of the mass spectrometer for the CO pulses showed a consumption in the catalysts in the first peaks accompanied by the production of H_2 (Figure S11) which has been attributed to the interaction of CO and OH groups that remained on the material, by the following reaction[88]:

$$CO_{ads/g} + OH_{support} \rightarrow CO_2 + \frac{1}{2}H_2 \qquad \text{Equation S 1}$$

While for O_2 chemisorption a slight production of water is observed due to oxidation (Figure S12).

Figure S11.

MS response for CO pulses and H_2 production in chemisorption.

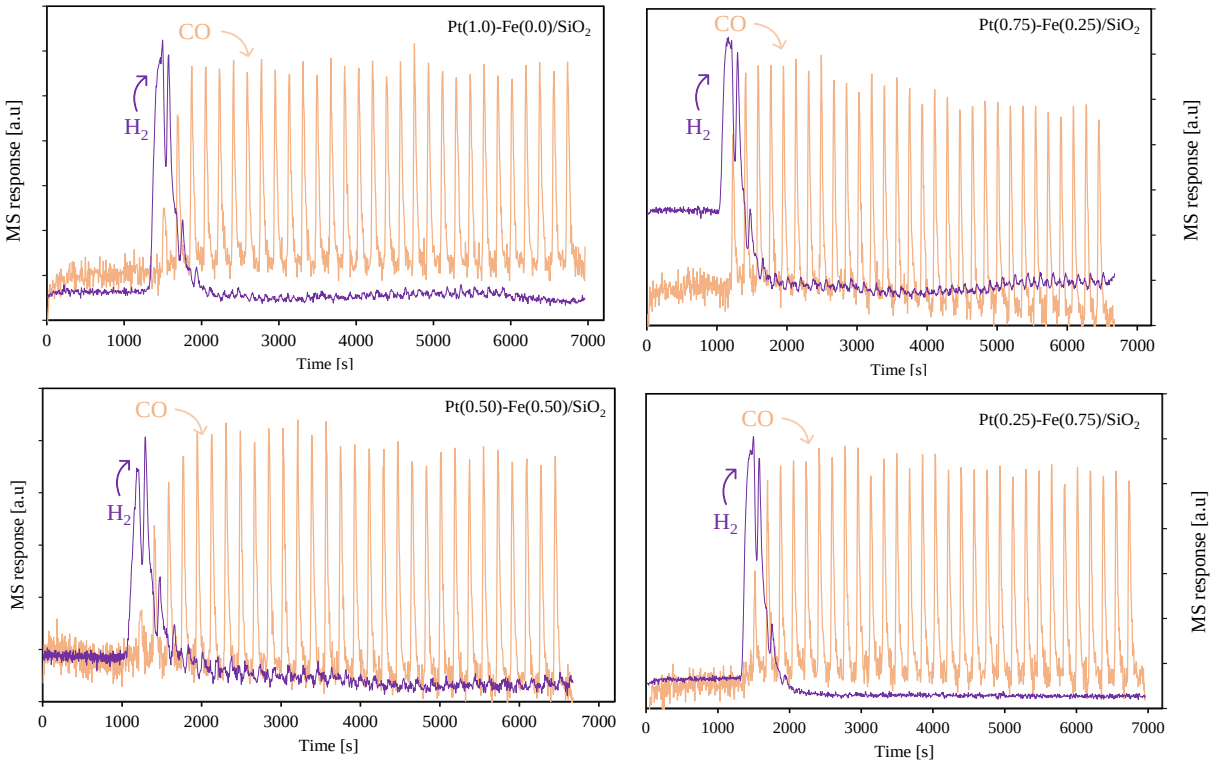

Figure S12.

MS response for O_2 pulses and H_2O production in chemisorption

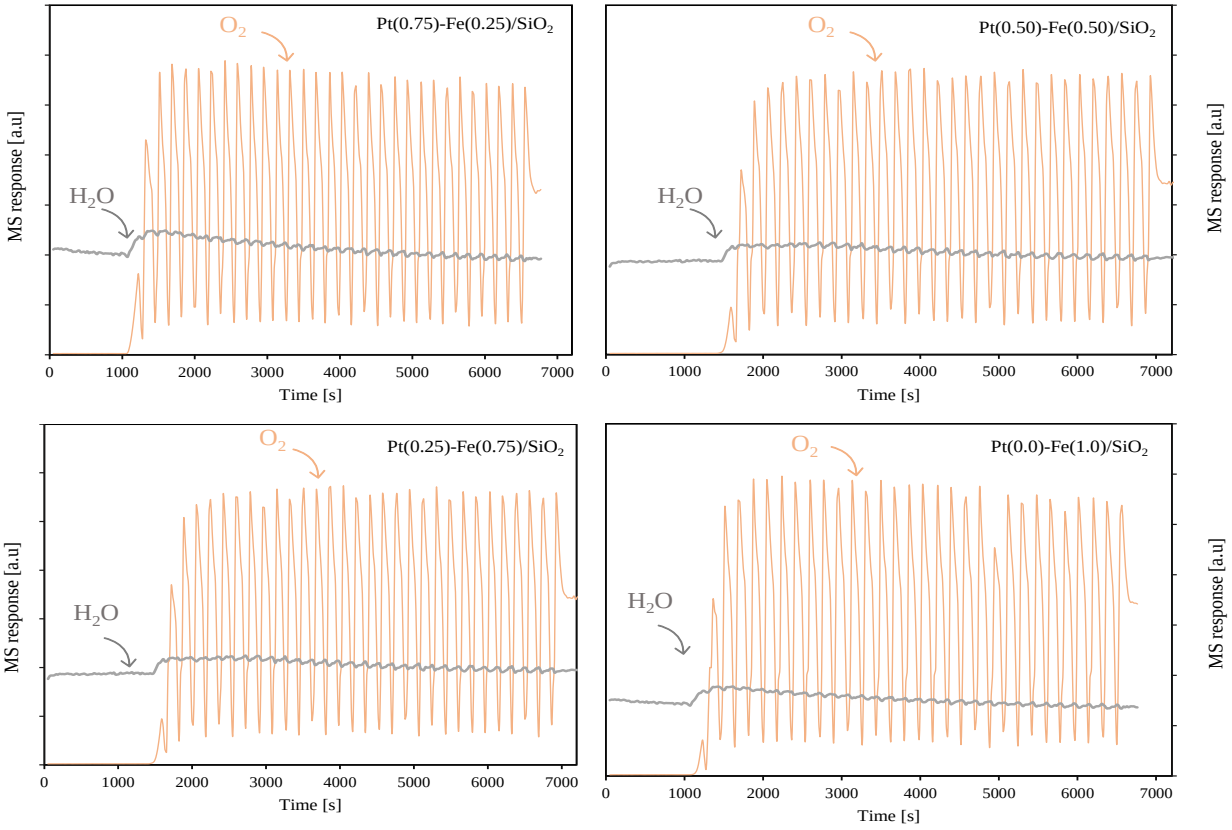

Appendix D. Catalytic test

System calibration. In all cases 4 known gas compositions were measured through the gas chromatograph. Below are the calibration curves for the gases involved in methane combustion.

Figure S13.

Calibration curves for each of the gases involved in methane combustion.

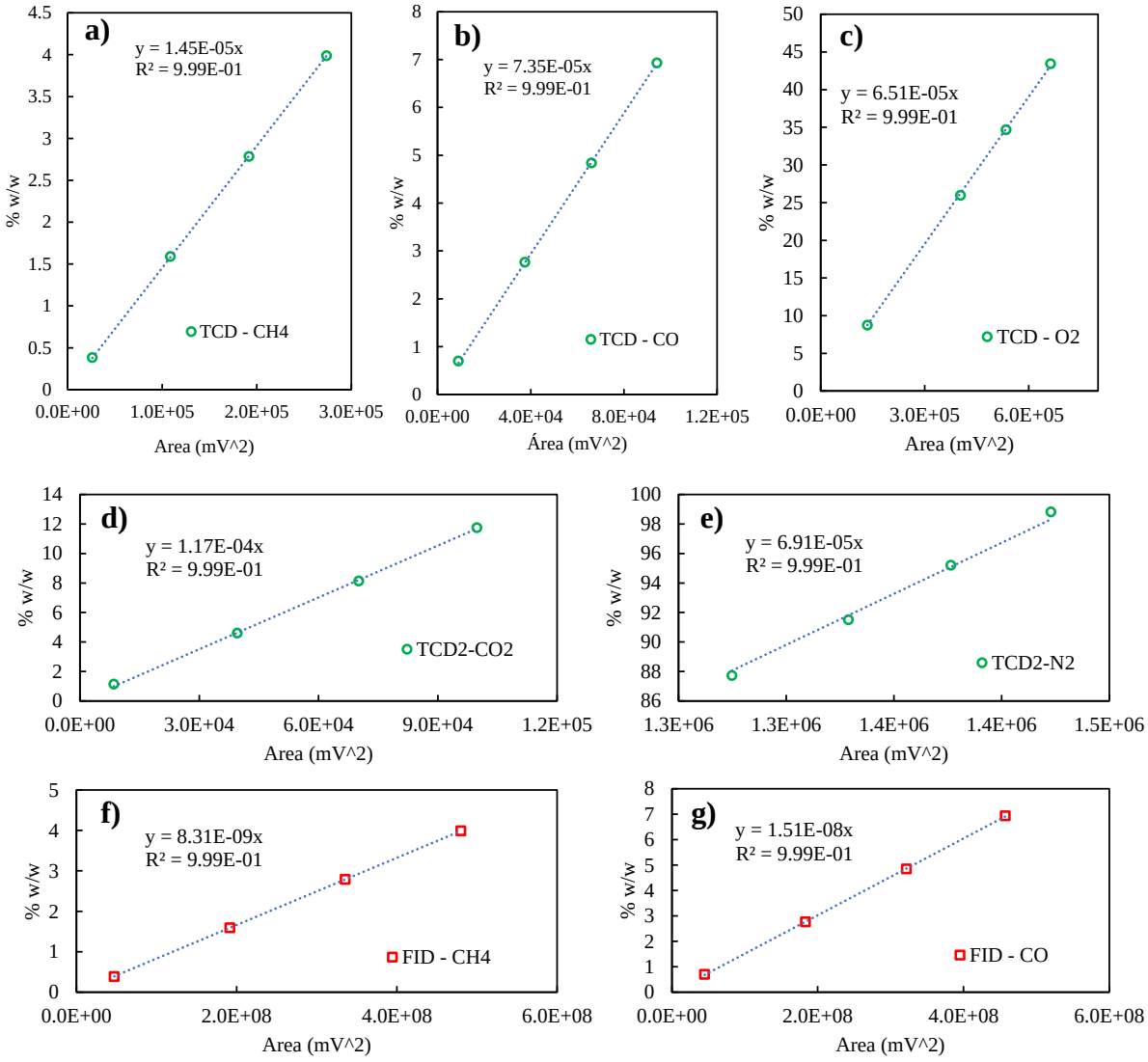

Note: a) Methane in TCD detector; b) Carbon monoxide in TCD detector; c) Oxygen in TCD detector; d) Carbon dioxide in TCD2 detector; e) Nitrogen in TCD2 detector; f) Methane in FID detector; g) Carbon monoxide in FID detector.

Preliminary tests for ruling out transport limitations

The conditions necessary to guarantee the absence of mass transport limitations were determined by applying the methodology proposed by Kiakalaieh *et al*[89]. The catalyst selected for these reactions will be the one with the highest porosity, that is, the smallest average pore size, in this case there is no significant difference in the area of the catalysts, so the experiments were carried out with the monometallic catalyst Pt(1.0)-Fe(0.0)/SiO_2-1. The reactions were carried maintaining the stoichiometric ratio CH_4/O_2 in 1:2 at a temperature of 400 °C for 2 h. For ruling out intraparticle transport limitations, the particle diameter (Dp) of the catalysts was modified in ranges of <100mm, 180-300mm, 100-600 mm and >800mm while the weight of the catalyst and the partial pressure of CH_4 were constant in 40 mg and 3.9 kPa, respectively. For rule out transport limitations between particles, the weight of the catalyst was changed with values of 20, 25, 35, 40 and 50 mg while both the diameter of the particles and the partial pressure of CH_4 were kept constant at 180-300 mm and 3.9 kPa, respectively. Figure S14 shows the linear trend of methane conversion from 20 to 50 mg of catalyst. On the other hand, the change in the diameter of the particles did not affect the conversion of methane. Then, it is possible to affirm that under these conditions the system is free from internal and external mass diffusion limitations[89,90].

Figure S14.

Results in terms of methane conversion for transport limitations.

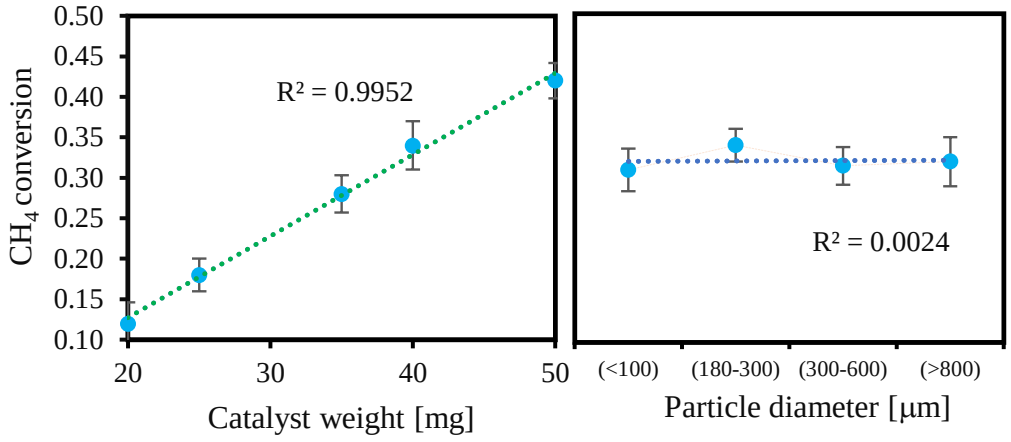

Monitoring of methane combustion reactions

For replica 1, the methane conversion at high temperatures values are presented as a function of time and temperature (Figure S15) and Table S6 shows the averages for the conversion of methane and oxygen and the carbon balance during the light off tests.

Figure S15.

Methane conversion at high temperature as a function of time and temperature.

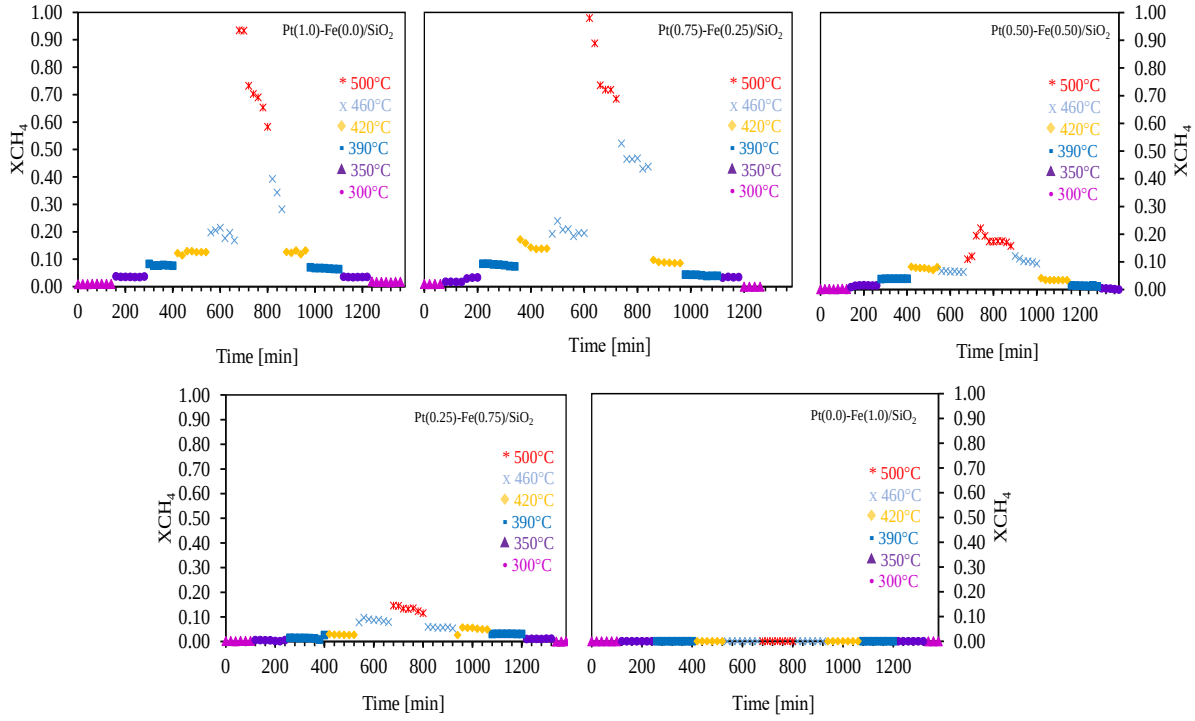

Note: For each catalyst, the results for the first synthesis replica are presented. The reactions were carried maintaining the stoichiometric ratio CH_4/O_2 in 1:2, the particle diameter used was between 180-300 mm and WHSV of 35 $Lg^{-1}h^{-1}$. The CH_4, O_2 and N_2 fluxes were constant with values of 0.4460, 0.8920 and 3.5680 mmol/min, respectively.

Figure S15 shows the decrease in methane conversion as the platinum fraction in the catalysts decreases, until there is no activity for the monometallic iron catalyst for the temperatures studied**.** In the same way, an apparent stability at low temperatures is evident. This is confirmed in Figure S16 which shows the conversion of methane at low temperatures as a function of time and temperature.

Table S6.

Methane conversion, oxygen conversion and carbon balance for testing catalysts in methane combustion. The values presented correspond to the Light off stage. Replica corresponds to the synthesis group of the catalyst.

		Replica 1			Replica 2			Replica 3		
Sample	T	X_{CH4}	X_{O2}	Carbon balance	X_{CH4}	X_{O2}	Carbon balance	X_{CH4}	X_{O2}	Carbon balance
Pt(0.0)Fe(1.0)/SiO_2	300	0.000	0.000	-	0.000	0.000	-	-	-	-
	350	0.000	0.000	-	0.000	0.000	-	-	-	-
	390	0.000	0.000	-	0.000	0.000	-	-	-	-
	420	0.000	0.000	-	0.000	0.000	-	-	-	-
	460	0.000	0.000	-	0.000	0.000	-	-	-	-
	500	0.000	0.000	-	0.000	0.000	-	-	-	-
Pt(0.25)Fe(0.75)/SiO_2	300	0.003	0.008	0.99	0.004	0.009	1.01	-	-	-
	350	0.011	0.011	1.00	0.013	0.014	1.00	-	-	-
	390	0.031	0.028	1.00	0.028	0.025	0.99	-	-	-
	420	0.054	0.048	1.00	0.048	0.045	1.00	-	-	-
	460	0.086	0.080	1.01	0.082	0.08	1.00	-	-	-
	500	0.133	0.123	1.01	0.145	0.135	1.01	-	-	-
Pt(0.50)Fe(0.50)/SiO_2	300	0.003	0.006	1.01	0.002	0.004	1.00	0.003	0.005	1.00
	350	0.015	0.017	1.00	0.021	0.023	1.00	0.014	0.015	1.00
	390	0.039	0.040	0.99	0.042	0.043	1.00	0.036	0.037	1.01
	420	0.078	0.077	1.00	0.083	0.082	0.99	0.079	0.077	1.00
	460	0.105	0.104	1.00	0.120	0.131	1.00	0.110	0.111	0.99
	500	0.170	0.181	0.99	0.176	0.190	1.00	0.175	0.183	1.00
Pt(0.75)Fe(0.25)/SiO_2	300	0.010	0.010	1.00	-	-	-	0.010	0.012	1.00
	350	0.034	0.031	1.00	-	-	-	0.033	0.031	1.00
	390	0.080	0.075	1.00	-	-	-	0.091	0.087	1.00
	420	0.148	0.142	1.00	-	-	-	0.144	0.139	1.00
	460	0.205	0.197	1.00	-	-	-	0.211	0.199	1.00
	500	0.787	0.766	0.99	-	-	-	0.811	0.801	0.99
Pt(1.0)-Fe(0.0)/SiO_2	300	0.010	0.011	1.00	0.010	0.010	1.00	-	-	-
	350	0.036	0.034	0.99	0.038	0.035	1.00	-	-	-
	390	0.078	0.075	1.00	0.081	0.079	1.00	-	-	-
	420	0.124	0.119	0.99	0.132	0.122	0.99	-	-	-
	460	0.193	0.190	1.01	0.212	0.221	1.00	-	-	-
	500	0.774	0.742	1.00	0.791	0.769	1.00	-	-	-

Note: The catalyst without platinum fraction showed no activity. The values shown correspond to the averages recorded during the reaction time (3h for each temperature).

Figure S16.

Methane conversion at low temperature as a function of time and temperature.

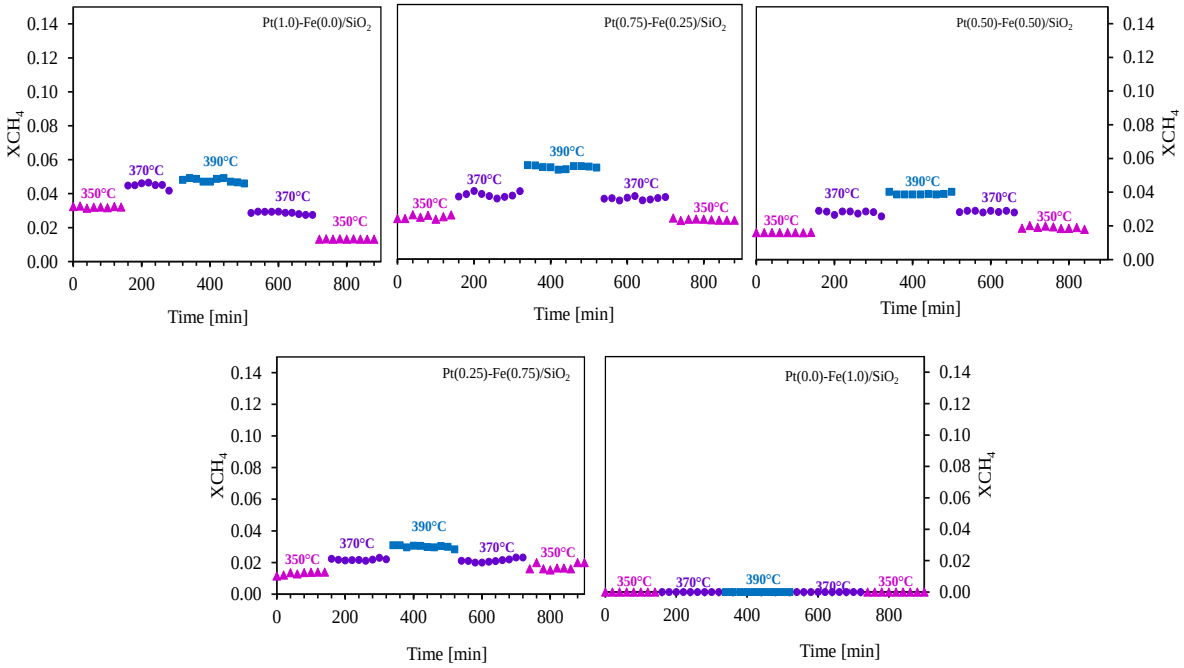

Note: For each catalyst, the results for the first synthesis replica are presented. The reactions were carried maintaining the stoichiometric ratio CH_4/O_2 in 1:2, the particle diameter used was between 180-300 mm and WHSV of 35 $Lg^{-1}h^{-1}$. The CH_4, O_2 and N_2 fluxes were constant with values of 0.4460, 0.8920 and 3.5680 mmol/min, respectively.

Temperature control behavior

As shown in Figure S 17, the exothermicity of the reaction for catalysts with a high platinum fraction generated a decrease in temperature in the control system, whose setpoint was 500 ° C, while Pt (0.25)Fe(0.75)/SiO_2 and Pt(0.50)Fe(0.50)/SiO_2 did not show these temperature jumps during the reaction. This behavior would explain the apparent deactivation of the catalysts.

Figure S17.

Comparison between the catalytic bed temperature and the temperature ramp set for the reaction

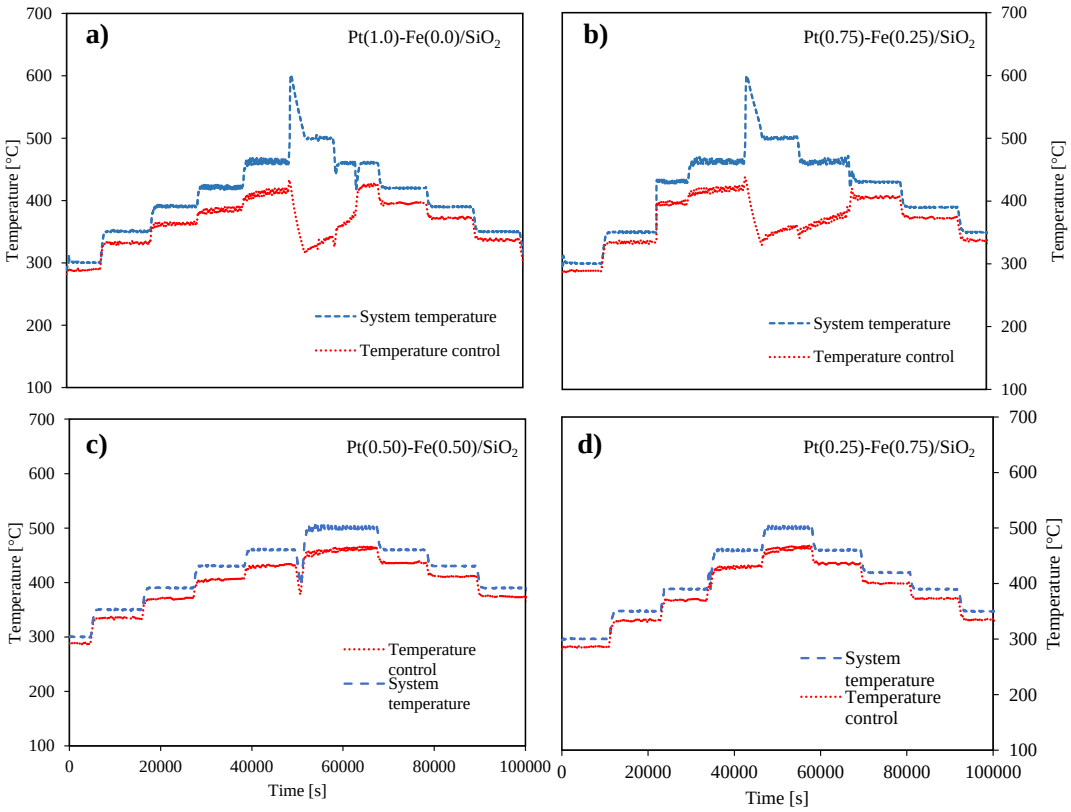

Activation energies analysis

The Arrhenius graph points to the equality in the apparent activation energy for the bimetallic catalysts. To corroborate this hypothesis, the calculation of the relative error was carried out considering that the division of a pair of parallel lines must be equal to 1. The results are shown in Table S7. The maximum error found is 5%.

Table S 7.

Ea_{app} values and parallelism calculation

Sample	Ea_{app} [kJ mol^{-1}]*	Ea_1/Ea_2	%Error**
Pt(0.0)-Fe(1.0)/SiO_2	-	-	-
Pt(0.25)-Fe(0.75)/SiO_2	70.94	1.04	4.05
Pt(0.50)-Fe(0.50)/SiO_2	68.16	1.02	1.74
Pt(0.75)-Fe(0.25)/SiO_2	67.01	1.05	5.02
Pt(1.0)-Fe(0.0)/SiO_2	57.87	-	-

*Ea_{app} was calculated multiplying the slope of the Arrhenius plot by the gas constant (8.314 J/ molK)

**The error was calculated considering that the division of a pair of parallel lines must be equal to 1.

Characterization after reaction

Figure S18.

H_2-TPR in terms of water production to catalysts after reaction at 350 and 500 ° C

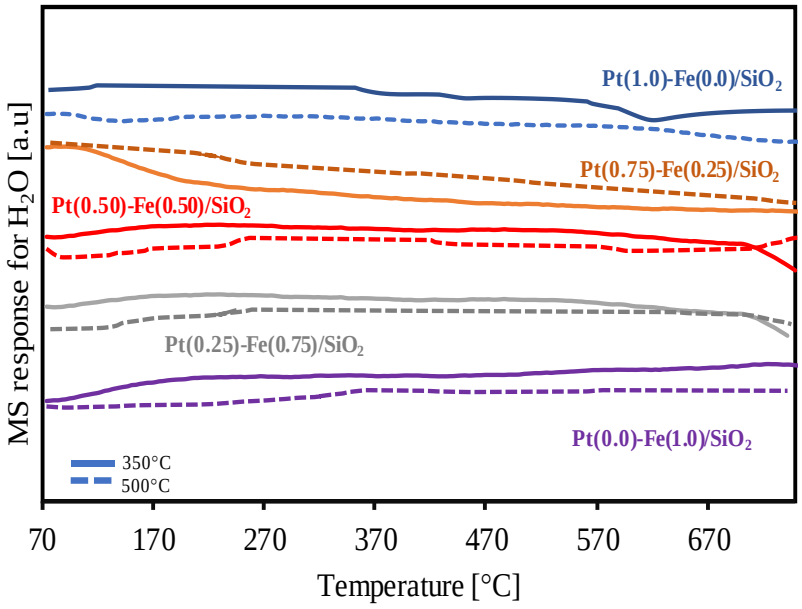

Appendix E. Statistics

Differences between selectivities- ANOVA

Two factors were studied, 1) Temperature; 2) Sample - metal fraction in catalysts. For the analysis the results for the Pt(0.0)-Fe(1.0)/SiO_2 catalyst were not considered.

Table S8.

Contingency table, CO_2 selectivity results.

	Sample				
Temperature [°C]	Pt(0.0)-Fe(1.0)/SiO_2	Pt(0.25)-Fe(0.75)/SiO_2	Pt(0.50)-Fe(0.50)/SiO_2	Pt(0.75)-Fe(0.25)/SiO_2	Pt(1.0)-Fe(0.0)/SiO_2
350	0	0.982	0.989	0.994	0.995
370	0	0.994	0.996	0.998	0.998
390	0	0.997	0.998	0.999	0.999

Before ANOVA, it was verified that the residuals followed a normal distribution of the data. Since the data fit with 99.18% to a linear regression (Figure S18), these assume a normal distribution.

Figure S19.

Residual normality test

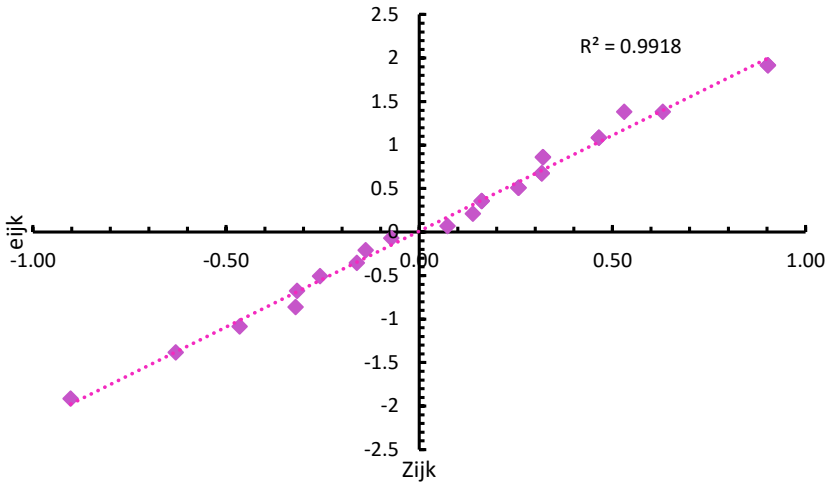

The interaction graphs (Figure S19) allow us to find possible effects produced by the relationship between the factors. In this case the lines appear to be parallel and there are no cuts between them. This interaction effect indicates that there is no relationship between the temperature and the catalyst, so it is possible to analyze the individual effects for each factor.

Figure S20.

Interaction graphics. a) With respect to temperature; b) Regarding the catalyst

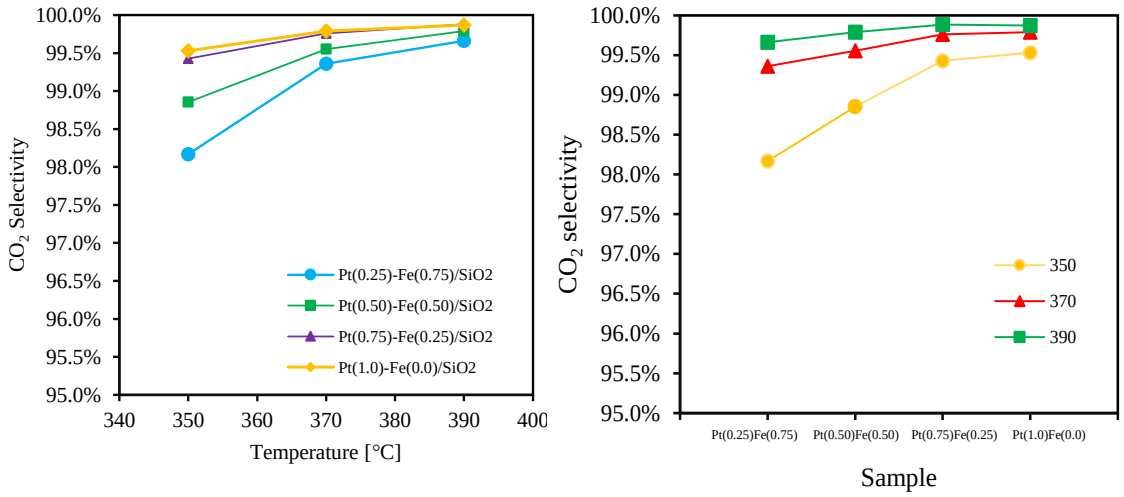

Table S8 shows the results of the ANOVA test. The -p value is compared with the level of significance, finding that there is an effect of temperature on CO_2 selectivity, so that for at least one of the temperatures the results presented differences, while for the type of catalyst it is considered that there is no difference in the results.

Table S9.

ANOVA table of CO_2 selectivity.

Source of variations	SS	Df	MS	F	p-value	F crit
Temperature	0.0001425	2	7.13E-05	9.112	0.015	5.143
Sample	0.0000863	3	2.88E-05	3.679	0.082	4.757
Error	0.0000469	6	7.82E-06			
Total	0.0002758	11				

Note: SS: Sum of squares; Df: degrees of freedom; MS: mean of squares; F: F-statistic; p-value: is the probability of obtaining test results at least as extreme as the results observed; F crit: It is the F value associated with the level of significance of 0.05.

The means comparison tests that are applied after a significant ANOVA are based on the calculation of confidence limits for said means. One of the most used is the Tukey test. This test will allow us to know which of the groups within a factor is

significantly different from the others. Its application in this case provides the following ranges:

Table S10.

Results of the Tukey test applied after analysis of variance.

Groups to compare	N	Difference	T -student	Lower limit	Upper limit
350-370	5	0.0062	2.18	0.0023	0.0100
370-390*	5	0.0018	2.18	-0.0020	0.0056
350-390	5	0.0081	2.18	0.0042	0.0119

Note: Means significantly different from each other (α= 0.05).

The intervals containing 0 correspond to group means (treatments) that are not significantly different from each other. In this case, it was found that the higher temperatures are equal while the difference occurs at 350 ° C.